Kobe University Repository : Kernel

PDF issue: 2025-12-04

Changes in dissolved organic matter composition and dynamics in a subtropical mangrove river driven by rainfall

Kida, Morimaru ; Tanabe, Mai ; Tomotsune, Mitsutoshi ; Yoshitake, Shinpei ; Kinjo, Kazutoshi ; Ohtsuka, Toshiyuki ; Fujitake, Nobuhide

(Citation)
Estuarine, Coastal and Shelf Science,223:6-17

(Issue Date)
2019-07-31

(Resource Type)
journal article

(Version)
Accepted Manuscript

(Rights)
© 2019 Elsevier Ltd. All rights reserved.
This manuscript version is made available under the CC-BY-NC-ND 4.0 license
http://creativecommons.org/licenses/by-nc-nd/4.0/

(URL)
https://hdl.handle.net/20.500.14094/90007896

Changes in dissolved organic matter composition and dynamics in a subtropical mangrove river driven by rainfall

Journal: Estuarine, Coastal and Shelf Science

Morimaru Kida[1†‡*], Mai Tanabe[1], Mitsutoshi Tomotsune[1¶], Shinpei Yoshitake[2¶] Kazutoshi Kinjo[3], Toshiyuki Ohtsuka[4], and Nobuhide Fujitake[1]

1 Graduate School of Agricultural Science, Kobe University, 1 Rokkodai, Nada, Kobe, Hyogo 657-8501, Japan

†Research Fellow of Japan Society for the Promotion of Science

2 Takayama Field Station, River Basin Research Center, Gifu University, 919-47, Iwai, Takayama, Gifu 506-0815, Japan

3 Faculty of Agriculture, University of the Ryukyus, 1 Senbaru, Nishihara, Nakagami, Okinawa 903-0213, Japan

4 River Basin Research Center, Gifu University, 1-1 Yanagito, Gifu, Gifu 501-1193, Japan

‡ Present address: Research Group for Marine Geochemistry (ICBM-MPI Bridging Group), Carl von Ossietzky University of Oldenburg, Institute for Chemistry and Biology of the Marine Environment (ICBM), Carl-von-Ossietzky-Str. 9-11, 26129 Oldenburg, Germany

¶ Present address: Faculty of Education and Integrated Arts and Sciences, Waseda University, 2-2 Wakamatsu, Shinjuku, Tokyo 162–8480, Japan

***Corresponding author**: Morimaru Kida

Institutional address: m.kida@people.kobe-u.ac.jp

Private address: marumori1004@gmail.com

Tell: 078-803-5846

ORCID ID: 0000-0002-9908-2012 (M.K.)

Abstract

Dissolved organic matter (DOM) plays an important role in sustaining ecosystem services of mangrove forests through well-described biogeochemical and ecological functions. This study was conducted in the Fukido River (Ishigaki Island, Japan) to better understand the seasonal and episodic changes in DOM concentration and composition in a subtropical mangrove system. Water samples were collected seasonally along a headwater–mangrove–sea transect on 10 occasions from September 2014 through June 2016. DOM was fractionated based on hydrophobicity into two fractions (hydrophobic and hydrophilic) and also analyzed by excitation-emission matrix spectroscopy combined with parallel factor analysis (PARAFAC). Although seasonal changes in DOM concentration and composition were not observed, both hydrophobic and hydrophilic DOM concentrations and levels of the identified three PARAFAC components clearly increased during a typhoon event. It is suggested that episodic increases in freshwater input due to a typhoon caused enhanced leaching of DOM from mangrove litter and dissolution of mangrove soil organic matter (SOM), which was otherwise retained in the mangrove soil by salinity-induced aggregation. The aggregation–dissolution properties of SOM are crucial in determining the magnitude of DOM outwelling and possibly SOM accumulation rate by enhancing advective DOM exchanges. Future studies are needed to evaluate the size of the carbon pool and outwelling of DOM after classifying mangrove forests based on the hydrological regime that influences biogeochemical conditions in the forests.

Keywords: Aggregation; Blue carbon; DOM; Dissolution; Hydrological regime; SOM

Regional Index Terms: Japan, Okinawa, Ishigaki, Fukido

1 Introduction

Mangrove forests act not only as a large C pool but also as a source of organic matter into the ocean. This is a combined result of their geographical location between land and sea, their large C pool per unit area and organic matter transportation by rivers and tides (Alongi, 2014). Traditionally, it was thought that outwelling of litter from coastal wetlands is a major direct source of energy for the secondary production of estuaries and nearshore waters (Lee, 1995; Odum, 1968). This "outwelling hypothesis" is now considered mostly restricted to the direct vicinity of mangrove forests (Kristensen et al., 2008). One of the primary reasons for this is decomposition of litter to dissolved organic matter (DOM). The litter decomposition takes place with an initial rapid stage (within the first weeks after litter fall) and a later slow stage, and in the initial stage litter can lose up to 60% of its initial weight mainly by DOM leaching (Benner et al., 1990; Wafar et al., 1997). The leached DOM is much more dynamic than litter and will be exported to coastal and even offshore waters, while undergoing photo- and bio-degradation. As a consequence, mangrove DOM can account for as much as 10% of the global transport of terrestrially-derived, refractory DOM to the ocean (based on the global mangrove areal estimate in 2006) (Dittmar et al., 2006).

The role of mangrove forests as a large source of DOM to support the coastal ecosystems is an important topic in mangrove research, and the number of relevant studies has been increasing since 2000 (Cawley et al., 2014; Dittmar et al., 2006, 2001; Maie et al., 2012). A recent study has reported that DOM accounts for >90% of organic matter exported from mangrove forests to the sea (Ray et al., 2018). DOM is a highly heterogeneous collection of organic compounds that collectively play an essential role in key ecosystem processes such as attenuating sunlight and harmful UV radiation (Bricaud et al., 1981), influencing key trace metal speciation (Gledhill and Buck, 2012), and modification of bacterial metabolism (Tranvik, 1992). One of the approaches to fractionate DOM into ecologically meaningful fractions is separation into hydrophobic (HPO) and hydrophilic organic matter (HPI) based on the relative hydrophobicity (Thurman & Malcolm, 1981). HPO, of which main constituents are humic substances (Imai et al., 2001), is the primary metal-binding components in DOM owing to its carboxylic and phenolic functional groups (Blazevic et al., 2016). For example, complexation with iron is essential for oceanic primary productivity; through complexation, HPO can solubilize

74 iron, which would otherwise precipitate and become unavailable for the primary producers in neutral-pH, high-
75 salinity seawater (Gledhill and Buck, 2012). In contrast, HPI, which contains biogenic substances such as
76 proteins, lipids, amino acids, and carbohydrates, is generally biodegradable and can be more easily utilized by
77 heterotrophic bacteria to provide energy and biogenic elements such as C, N, P, and S (Tranvik, 1992). Since
78 HPO and HPI may respond differently to changes in hydrological and biogeochemical conditions and serve
79 different ecological functions, it is essential to examine these DOM fractions independently.

80 Mangrove forests have characteristic physical forces that drive advective groundwater DOM dynamics
81 (Santos et al., 2012). Since groundwater solute concentrations are often higher than overlying waters, these
82 forces can be a source of solutes (DOM, dissolved inorganic carbon, and nutrients) to overlying waters (Santos
83 et al., 2012). Although these forces can exert a major control on the biogeochemistry of sediments and overlying
84 waters, sediment biogeochemistry itself can also affect the magnitude of the advective DOM flux by changing
85 DOM solubility (Kida et al., 2017). The aggregation–dissolution properties of soil organic matter (SOM) due
86 to changes in salinity may be a key mechanism influencing DOM dynamics in mangrove forests. We recently
87 proposed that, in the Fukido mangrove forest, Japan, SOM was accumulated in the soil because of the
88 immobilization of SOM and/or SOM-clay complexes under saline conditions, which serves as one of the
89 mechanisms underlying SOM accumulation in mangrove soils (Kida et al., 2017). This proposition was based
90 on the observation that sequential washing with freshwater (and the corresponding decline in salinity) caused
91 dissolution of SOM from the mangrove soil, but sequential washing with artificial seawater did not. The same
92 phenomenon was also found for soil samples from a Trat mangrove forest, Thailand, irrespective of mangrove
93 species (Kida et al., not published). This finding implies that if sedimentary salinity decreases sufficiently to
94 cause SOM dissolution, for example by an episodic increase in freshwater input due to a typhoon, DOM can be
95 exported by advective exchanges at a higher level than usual. Although this speculation is in line with various
96 literature reporting higher mangrove contribution to DOM in mangrove rivers during rainy seasons and/or
97 episodic rain events (e.g., Cawley et al., 2014), it has not yet been proven in a field study.

98 In this study, we conducted HPO/HPI fractionation along with optical measurements (ultraviolet [UV]-
99 visible absorption spectroscopy and excitation-emission matrix spectroscopy [EEM]) to better understand the

seasonal and episodic changes in DOM concentration and composition along a headwater–mangrove–sea transect in the Fukido mangrove, which was located at the northern limit of mangrove habitats. Particular emphasis was given to elucidating influences of a typhoon event on the surface water DOM dynamics and on the exchange of DOM with the mangrove soil. Optical measurements allow for inexpensive and high sample throughput measurements and require small volumes of water. Optical parameters derived from such measurements have been linked to DOM quality, composition, and biogeochemical processing (Helms et al., 2008; Huguet et al., 2009; McKnight et al., 2001; Spencer et al., 2012; Weishaar et al., 2003) and thus have the potential to improve our understanding of DOM dynamics in complex aquatic environments, like mangrove rivers.

2 Materials and Methods

2.1 Study site and sampling

The study was conducted in the Fukido River, which passes through a mangrove forest on Ishigaki Island, Okinawa, Japan (Fig. 1a). The climate on Ishigaki Island is subtropical, with an annual mean temperature of 24.3°C and annual precipitation of 2,107 mm. Precipitation in May to October is relatively larger than the rest of the year, mainly due to typhoons, accounting for 60% of the annual precipitation, with August and September each having approximately twice as much monthly precipitation as December to March (between 1981 and 2010, Ishigakijima Local Meteorological Observatory [ILMO], Fig. 1b). Broadleaf forests occupy about 95% of the watershed (2.38 km^2, excluding the mangrove forest) with the rest of land use being sparse sugar cane and paddy fields (0.11 km^2), and the river is subject to little human activity. The soil in the catchment is red-yellow soil with a thin A horizon and a low SOM content, which is common in subtropical and tropical areas with high SOM biodegradation rates. The Fukido mangrove forest is a small (0.19 km^2, estimated by Google Earth Pro) mangrove forest vegetated by *Rhizophora mucronata* and *Bruguiera gymnorrhiza* and is registered as a national park. A detailed study of species composition, biomass, and aboveground net primary productivity of this mangrove forest has been reported elsewhere (Ohtsuka et al., 2019). Respiratory mangrove roots protrude from the soil surface and there is no understory and litter layer. The forest soil is mineral rather than peaty (sand

contents of 60%–70%) and has a depth of about 1 m before the bedrock. The tentative soil type is gley soil, and a soil organic carbon content does not change systematically with depth and vary between 2% and 5% (Kida et al., not published). There are many notable burrowing macro fauna, such as fiddler crabs (*Uca dussumieri, U. vocans,* and *U. tetragonon*), soldier crabs (*Scopimera globose*, *Mictyris brevidactylus)*, and mud shrimps (*Thalassina anomala*). Their burrows could serve as storage points and batch reactors for DOM production (Maher et al., 2013; Stieglitz et al., 2013). The Fukido River is short (<1.5 km) and has an area of 0.015 km^2 (7.9% of the mangrove forest) within the mangrove forest. The Fukido River has a clear semidiurnal tide (two tidal cycles per day) within the mangrove forest, with maximum tidal height reaching more than 1 m during spring tide (Ohtsuka et al., 2019). Owing to its small size, the Fukido River is ideal for whole-system water sampling.

Surface water samples were collected along a headwater–mangrove–sea transect at seven points as shown in Fig. 1. They were directly collected in 280-mL volume transparent polyethylene terephthalate bottles after rinsing more than three times with the collected water. Preliminary experiments found that DOC contamination from the bottles in the time course of up to nine months was under the detection limit of the total organic carbon analyzer used (<0.05 mgC L^{-1}). A total of 68 samples were collected approximately seasonally on 10 occasions from September 2014 through June 2016 (Table 1, Fig. 2). The pH and salinity (*S,* Practical Salinity Scale) measurements were conducted in situ with portable meters (LAQUAtwin series, HORIBA, Japan). The pH values ranged 7.1–8.3 and generally increased towards downstream areas (Table 1). All sampling was conducted at low tide when outwelling of mangrove-derived materials would be highest (Dittmar et al., 2001), but differed in the extent of rainfall effect (baseflow or not). The baseflow condition was defined as any period more than 24 h after a rain event (7 out of the 10 occasions were under the baseflow condition). On 24–26 August 2015, successive three-day sampling was conducted to capture the changes in DOM concentrations and compositions caused by heavy rain due to a typhoon, named Goni (Category 4 according to the Saffir–Simpson Scale). The typhoon passed through Ishigaki Island at around 20:00 on 23 August 2015. The precipitation on 23, 24, 25 and 26 August was 241, 33, 54 and 14 mm, respectively (ILMO). Samples were kept cooled in the dark during transportation back to the laboratory and filtered within 24 hours of collection

with a water- and sample-cleaned glass fiber filter (ADVANTEC GF-75, nominal pore size of 0.3 μm). Carbon contamination from the filter was negligible (<0.01 mg C L^{-1}) according to this protocol. The exception was the series of samples collected during the typhoon event, which was filtered within 1–2 days of collection. The filtered samples were stored in the dark at 4°C and analyzed within one week of collection.

Groundwater collection was conducted on 8 March 2016 by a soil water sampler (DIK-8392, Daiki Rika Kogyo, Saitama, Japan) every 2 h for 24 h, thus covering two tidal cycles. Five 1-m vinyl chloride pipes with a porous ceramic cup (18 × 60 mm) attached at the head were inserted to a depth of 20, 40, 60, 80, and 100 cm with care not to disturb soil, and groundwater (50 mL each) was collected by syringe. It took about 30 min per sampling to fill the syringe with groundwater. We also attempted to collect groundwater during the typhoon event at a place closer to the sea than on 8 March 2016 (Fig. 1). However, because of the difficulties of monitoring during the massive typhoon, we could only collect groundwater samples a few days after the typhoon (26–27 August 2015). The sampling settings were almost identical to the 8 March 2016 groundwater sampling (i.e., 20, 40, 60, and 80 cm depth every 2 h for 30 h). The groundwater samples were transported, prepared, and analyzed the same way as surface water samples.

2.2 DOM fractionation

The water samples were fractionated into HPO and HPI as described by Tsuda et al. (2012). The validity of the method for samples with different salinities was previously confirmed (Kida et al., 2016). Briefly, 0.4 mL of purified DAX-8 resin (ground to 50–200 μm) was weighed into a glass vial with a Teflon screw cap, and 20 mL of the sample was added and acidified with 1 mL 1M H_2SO_4 (special grade, Wako, Japan) to adjust the pH to <2. After shaking for 24 h, the dissolved organic carbon (DOC) concentration of the supernatant, the HPI fraction, was analyzed after filtration through a GF-75 glass fiber filter. The HPO concentrations were calculated as the difference between the bulk DOC concentration and the HPI concentration. Organic C contamination from the system was determined with ultrapure water as a blank and used for correction (<0.1 mg C L^{-1}). Both the blank determination and HPO adsorption were conducted in triplicate or quadruplicate, consuming <100 mL of each sample. The precision of the replicate measurements was 2.8% for the average

178 coefficient of variation (CV) of all the measurements, and the average values were used for data analysis and
179 are reported here. Although the DOM fractions retained on the DAX-8 resin can also include hydrophobic
180 neutrals, their contribution to DOM is generally very small in natural rivers (Imai et al., 2001), and thus we
181 assumed that the HPO fraction was almost exclusively occupied by humic substances. All glassware was acid-
182 washed and muffled at 450°C for more than 3 h before use to minimize possible contamination.

183 The DOC was measured as non-purgeable organic carbon in a total organic carbon analyzer (TOC-
184 L_{CPH}, Shimadzu, Japan) by the platinum-catalyzed high-temperature combustion method coupled to non-
185 dispersive infrared gas detection of CO_2. Each sample was first sparged with a carrier gas for 90 s in the built-
186 in syringe of the TOC analyzer after acidification to remove any inorganic C prior to combustion. Calibration
187 was performed by running four standards of a potassium hydrogen phthalate solution over an appropriate range
188 and one laboratory blank (ultrapure water). The elemental concentrations were calculated from the regression
189 line (coefficient of determination, $R^2 > 0.999$). Reported DOC concentrations are average values of triplicate
190 measurements. Samples were analyzed with repeated injections with the criteria that the peak area CV was
191 <2.0% or the SD was <0.2, whichever was lower. If the CV or SD exceeded the thresholds, up to two additional
192 analyses were performed and the most deviated outliers were eliminated.

193

194 **2.3 Optical measurements**

195 UV-visible absorption spectra (240–600 nm) were measured using a UV-visible spectrophotometer (V-630,
196 JASCO, Japan) with a 5-cm path length, acid-cleaned, quartz cuvette at ambient temperature. Measurements
197 were baseline-corrected using ultrapure water. The $SUVA_{254}$ was calculated by dividing the UV absorbance
198 (m^{-1}) measured at $\lambda = 254$ nm by the DOC concentration (mg C L^{-1}) and reported in L mg C^{-1} m^{-1}. The $SUVA_{254}$
199 was originally reported by Weishaar et al. (2003) to be correlated with percent aromaticity of isolated humic
200 substances and later used as a surrogate for DOM aromaticity in a number of studies. Although the presence of
201 Fe has been shown to influence $SUVA_{254}$ (Weishaar et al., 2003), a preliminary measurement with inductively
202 coupled plasma atomic emission spectrometry found that Fe concentrations in the Fukido River were low (under

203 the detection limit of the analyzer, 10 μgL^{-1}), and correction for Fe was not carried out. Napierian absorption
204 coefficients, $a(\lambda)$, of DOM were calculated as follows:
205 $a(\lambda) = 2.303A(\lambda)/l$
206 where $A(\lambda)$ is the measured absorbance at wavelength λ and l is the cell path length in meters (Hu et al., 2002).
207 Spectral slope ($S_{275–295}$), which has been related to apparent molecular weight and degree of photochemical and
208 microbial processing and used as a source differentiation (terrestrial vs marine) tool in estuarine studies (Fichot
209 and Benner, 2012; Helms et al., 2008), was calculated using a linear fit to the natural log-transformed $a(\lambda)$
210 spectrum in the ranges of 275–295 nm. Typically, a higher (steeper) $S_{275–295}$ value suggests a decrease in
211 molecular weight and aromaticity of DOM and an increase in the degree of photodegradation.
212 Fluorescence EEMs were collected with a spectrofluorometer (FP-6200, JASCO, Japan) equipped
213 with a 150 W xenon arc lamp at room temperature using 5 nm excitation and emission slit widths, a scan speed
214 of 500 nm min^{-1}, an excitation (Ex) range of 240–450 nm at 5 nm increments, and an emission (Em) range of
215 300–550 nm at 1 nm increments. The EEMs were measured for the samples collected after August 2015 (n =
216 42). Fluorescence signals were acquired in signal-to-reference mode to eliminate intensity fluctuations of the
217 xenon lamp. Excitation wavelengths below 265 nm were removed due to deteriorating signal-to-noise ratios.
218 Because inner filter effects (IFE) produce a suppression of 5% or more against true fluorescence intensity when
219 absorbance exceeds 0.042 (Kothawala et al., 2013), primary and secondary IFE corrections were applied to
220 each sample EEM using the absorbance of the corresponding sample in a 1-cm path length quartz cuvette
221 (Kothawala et al., 2013). The absorbance of all of the samples across the full EEM was less than 0.17.
222 Subsequently, an ultrapure water EEM measured on the same day as the samples was subtracted from each of
223 the IFE-corrected EEMs. Fluorescence intensities were normalized in Raman units (RU) using the Raman peak
224 measured at an excitation of 350 nm obtained from the ultrapure water EEM. We note that in Raman
225 normalization, the Raman peak was baseline corrected at an emission range of 371–428 nm, and only the Raman
226 peak area was used (corresponding to emission range of approximately 388–410 nm), as in Murphy (2011).
227 The biological index (BIX) was obtained from the corrected and Raman-normalized EEMs. The BIX
228 is calculated as the ratio of emission intensities at 380 nm and 430 nm (I380/I430) at an excitation of 310 nm

229 and estimates autochthonous biological activity in water environments (Huguet et al., 2009). High values (>1)
230 of BIX correspond to DOM of predominantly autochthonous origin and to freshly released DOM in water,
231 whereas lower values (0.6–0.7) correspond to low DOM production in natural waters (Huguet et al., 2009).
232 Although corrections for the effect of the instrument-specific response on EEMs were not applied because of
233 the lack of a manufacturer-provided correction factor, the trend for BIX values on DOM source interpretation
234 is robust (Huguet et al., 2009).
235
236 **2.4 PARAFAC analysis**
237 We analyzed the EEMs by parallel factor analysis (PARAFAC) to mathematically deconvolute them into
238 distinct fluorescent components with independent spectral characteristics. We used Matlab R2017b with the
239 *drEEM* toolbox (v 0.4.0) (Murphy et al., 2013). A sample set (n = 6), which was collected on 1 June 2015 when
240 precipitation of 17 mm was recorded, was included in the PARAFAC analysis (total of 48 samples). EEMs
241 were normalized to total fluorescence intensities to account for the differences in fluorescence intensity among
242 samples and reduce correlations between PARAFAC components. During the exploratory phase, eight outliers
243 were removed based on their leverage. The model was constrained to non-negative values. Models (3–5
244 components) were developed with a convergence criterion of 10^{-8}. Each model was iterated 10 times after
245 initializing with random starting values, and only the least squares solution was retained. The final three-
246 component model accounted for >98.8% of the measured spectral variation and had a core consistency value
247 of 53.4%. The appropriate component number was determined by residual analysis and split-half analysis
248 (S4C6T3; Murphy et al., 2013). The identified components were quantitatively compared with the published
249 data using an open-access spectral database (OpenFluor; Murphy et al., 2014). On OpenFluor, one can compare
250 fluorescence datasets and determine Tucker congruence coefficient (TCC) between pairs of excitation (TCC_{ex})
251 and emission (TCC_{em}) spectra. If an identified fluorescent component has a strong match ($TCC_{ex\times em} > 0.95$), it
252 means that the same or a spectrally indistinguishable validated component had been reported in the literature.
253 After the model building, the outliers were projected onto the validated model to obtain scores for them.
254 However, three out of the eight samples were not adequately modeled (judged by residuals), and thus their

PARAFAC results are not presented. The fluorescence intensity at the maximum for each component was represented by F_{max} (in RU) (Murphy et al., 2014). Although the EEMs in this study were not corrected for the instrument-specific bias, the PARAFAC results can be internally compared because they were obtained with the same instrument under identical conditions.

2.5 Data analysis

The percent contribution of DOM, HPO, HPI, and PARAFAC components from the mangrove forest were estimated according to Cawley et al. (2014). Briefly, the difference between the area under the conservative mixing line and the area under the measured data was divided by the area under the measured data and multiplied by 100 to get the percentage values. The data points were interpolated by 0.1 salinity increments. The conservative mixing line was determined by fitting a line between the headwater and sea samples on each day. On 10 November 2015 and 8 March 2016, the seawater sample collected on 20 June 2016 was used as a seawater endmember for PARAFAC components because the PARAFAC model was not well fitted to the seawater samples on these days. On 20 June 2016, the sample collected at the upper end of the mangrove forest was used as a river endmember because it had a lower DOC concentration than the headwater sample while having almost same salinity. In addition, on 25 and 26 August 2015, the seawater sample collected on 24 August 2015 was used as a seawater endmember because we could not collect a seawater endmember on these days because of dilution of seawater by intense rainfall (Table 1, Fig. 3). Our seawater endmembers were not a pure seawater end member because of relatively low salinity ($S < 32$), and thus this method likely conservatively estimates the mangrove contribution, assuming that seawater had lower DOM concentration and fluorescence intensity. A two tailed F-test (95% confidence level) was used to determine whether measurements were statistically different from the conservative mixing line.

Statistical analysis was carried out using Origin 2016 (OriginLab Corporation, MA, USA). Differences between DOC concentrations, the proportions of HPO in DOM (%HPO), or values of optical indices under the baseflow conditions and during the typhoon event were analyzed by the Student's t-test. The statistical difference between multiple parameters was tested by Tukey-Kramer's multiple comparisons of means when

the normality and homogeneity of variance was confirmed by Shapiro-Wilk test and Leven's test, respectively. A significance level of 0.05 was selected for the t-test and Tukey-Kramer's multiple comparisons to test the null hypothesis. Correlations between parameters were analyzed by linear regression analysis. Linear correlations were considered statistically significant when $P < 0.01$.

3 Results

3.1 DOM distribution along the salinity gradient

In the first year, we collected water samples seasonally from September 2014 (summer) to May 2015 (spring) (Table 1). The intention was to capture the seasonal changes in DOC concentrations and DOM compositions (i.e., %HPO). However, we did not observe significant seasonal changes (Tukey-Kramer, $P > 0.05$). A preliminary sampling on a heavy rainy day in May 2013 showed higher DOC concentrations and %HPO than under the baseflow conditions (Table S1). Therefore, in the second year, water sampling during a heavy storm event was planned. The expectation was that the changes in concentrations and compositions of DOM would be observed, allowing us to assess whether an episodic heavy rain event affects DOM dynamics. We successfully collected samples during a typhoon event on 24–26 August 2015 (Typhoon Goni, Fig. 2).

The DOM fractionation results are given in Fig. 3 with the HPO and HPI concentrations as well as DOM concentrations plotted against salinity (only data with PARAFAC results are shown for clarity; see Fig. S1 for other results). The DOM concentrations ranged between 0.67 and 3.71 mg C L^{-1}, while the HPO and HPI concentrations ranged from 0.29 to 2.34 mg C L^{-1} and 0.22 to 1.37 mg C L^{-1}, respectively. Both HPO and HPI showed positive deviations from conservative mixing, indicating that there were inputs of both HPO and HPI from the mangrove forest, although the non-conservative behavior of HPI was less pronounced than HPO. An exception was observed on 20 June 2016, when the headwater sample had a higher HPO and HPI concentration than a sample collected at the upper end of the mangrove forest. Nevertheless, under the baseflow conditions, on average 25% ± 13%, 22% ± 12%, and 15% ± 17% of DOM, HPO, and HPI were contributed from the mangrove forest to the Fukido River, respectively (Fig. 3, Table 3). On 24–26 August 2015, when the catchment had heavy rain due to Typhoon Goni, the DOC concentrations increased, especially at the headwater

307 and the second sampling point, compared with values under the baseflow conditions (2.48 ± 0.90 vs 1.20 ± 0.35
308 mg C L^{-1}, Table 1, $P < 0.001$), suggesting a supply of organic materials from the catchment and mangrove
309 forest. During the typhoon event, the DOC concentrations increased day by day for all sampling points except
310 for at the headwater. The sharp DOC increases at the sampling point located at the upper end of the mangrove
311 forest were most notable (Fig. 3, Table 1). Moreover, salinity decreased day by day despite the identical
312 sampling positions and timing (i.e., all at low tide), indicating that seawater was diluted by freshwater because
313 of the heavy rain, at least until the estuarine sampling point. During the typhoon event, 24% ± 3% and 29% ±
314 3% of DOM and HPI were contributed from the mangrove forest to the Fukido River, respectively (Fig. 3,
315 Table 3). The contribution of the mangrove forest to HPO was on the same order as to DOM and HPI, but it
316 was insignificant during the typhoon event ($P > 0.05$).

317 The proportions of HPO in DOM (%HPO), based on C concentrations, showed a similar trend along
318 the salinity gradient irrespective of sampling days (Fig. 4). The %HPO ranges were 33.6%–71.0% and
319 decreased with the increase in salinity. The highest and lowest %HPO were observed at the headwater and the
320 sea, respectively. The mean %HPO (±SD) at the headwater and the sea was 68.2% ± 2.1% and 46.7% ± 7.4%,
321 respectively. The mean %HPO at the headwater under the typhoon and baseflow conditions was 69.6% ± 1.1%
322 and 67.1% ± 1.5% and slightly higher during the typhoon event, although the difference was not significant (P
323 $= 0.055$).

324 Figure 5 shows groundwater DOC concentrations at different depths. The DOC concentrations of the
325 groundwater increased with depth and were ~3 times higher than the surface water DOC concentration
326 measured at the closest point during the low tide on the same day (1.18 mg C L^{-1}, Table 1). Although just a
327 snapshot, this implies that groundwater would necessarily be a source of DOC to the surface water of the Fukido
328 River if advective groundwater exchanges occurred.

329

330 **3.2 Optical parameters**

331 The distribution patterns of the measured optical parameters as well as %HPO are plotted against salinity in
332 Fig. 4. The $SUVA_{254}$ decreased with the increase in salinity as in %HPO, showing high values at the headwater

333 (3.1–4.2 L mg C^{-1} m^{-1}) and low values at the sea (0.8–3.0 L mg C^{-1} m^{-1}). The BIX values fluctuated between
334 0.55 and 0.76 until S = 15–20, then rapidly increased up to 0.93 at the sea sampling point. The $S_{275–295}$ varies
335 between 0.011 and 0.019 nm^{-1} and consistently increased along with salinity except for in November 2016
336 when seawater samples irregularly had a lower value than the corresponding estuarine sample. When comparing
337 values of the optical indices within the mangrove forest ($0.05 < S < 15$) under the baseflow and typhoon
338 conditions, $SUVA_{254}$ values were significantly lower (3.3 ± 0.3 versus 3.7 ± 0.3) and BIX values were higher
339 (0.67 ± 0.04 versus 0.61 ± 0.04) during the typhoon event than under the baseflow conditions ($P < 0.05$), which
340 was against our expectation. This could be partly explained by inputs of non-humic materials from the mangrove
341 forest canopy, which will be discussed later. At the same salinity range, the difference in %HPO during the
342 typhoon event and under the baseflow conditions was not significant ($P = 0.75$).
343
344 **3.3 PARAFAC components**
345 Three components were identified by PARAFAC analysis of the Fukido River samples (Fig. S2, Table 2). All
346 of the three components had fluorescence maxima at Em > 350 nm. The components were named according to
347 their rounded fluorescence emission maximum: C_{480}, C_{410}, and C_{380}. C_{480} was composed of two peaks with Ex
348 < 265 nm and 360 nm at Em 478 nm. The fluorescence of C_{410} was blue-shifted relative to C_{480} and had
349 fluorescence peaks at Em 409 nm with Ex < 265 nm and 325 nm. C_{380} had broad fluorescence peaks at
350 approximately Em 310–440 nm (highest at 380 nm) with Ex < 265 nm and 275 nm. The spectral shape of C_{380}
351 was not good, with the emission spectra extending to 550 nm, probably because of the low sample fluorescence
352 intensity and low signal-to-noise ratios of the spectrofluorometer in the UV-C region. Although the EEMs in
353 this study were not corrected for the instrument-specific bias, C_{480} and C_{410} had multiple strong matches
354 ($TCC_{ex\times em} > 0.95$) on OpenFluor (36 components for C_{480} and 14 components for C_{410}). Assignments of the
355 components are summarized in Table 2 with descriptions of each component provided in the literature. C_{480} has
356 been found in a wide range of environments and suggested as a ubiquitous, terrestrial humic-like component
357 with high aromaticity (Osburn et al., 2016; Yamashita et al., 2010). C_{410} has also been reported as a ubiquitous
358 humic-like component and suggested as both photo-labile and bio-available (Cawley et al., 2012; Stedmon and

359 Markager, 2005a; Yamashita et al., 2010). C_{380} had only three matching components with $TCC_{ex \times em} > 0.9$, and
360 they were reported as either a tryptophan-like component (Soto Cárdenas et al., 2017) or combination of several
361 components (including protein-like components) having similar excitation spectra with different emission
362 spectra (Murphy et al., 2018). Considering spectral characteristics and peak positions of C_{380}, this component
363 could be categorized as a combination of a protein-like component and UV-C humic component. We note that
364 the number of the identified PARAFAC components in this study may have been underspecified because of the
365 small sample size (n = 40) (Murphy et al., 2013, 2011; Stedmon and Markager, 2005a). Therefore, C_{380} may be
366 separated into a protein-like component and UV-C humic-like component if the sample size was increased.
367 These components are frequently reported to co-exist in the estuarine environment and river-influenced ocean
368 margins (Cawley et al., 2014; Maie et al., 2014; Yamashita et al., 2015, 2010), which could explain why the
369 PARAFAC analysis could not resolve these components.

370 The F_{max} of the two humic-like PARAFAC components (C_{480} and C_{410}) had a significant strong
371 correlation with DOC concentrations (both $R^2 = 0.87$, $P < 0.001$). Consequently, they showed very similar non-
372 conservative distributions as DOC concentration irrespective of sampling days, with high values (up to 0.47
373 RU under the baseflow conditions) within the mangrove forest, and strong decreases with salinity to values
374 ≤0.04 RU at the sea sampling point (Fig. 3). The positive deviations from conservative mixing suggest that
375 there were inputs of these humic-like components from the mangrove forest. C_{380}, in contrast, had a weaker
376 overall correlation with DOC concentrations ($R^2 = 0.79$, $P < 0.001$), and the relationship was particularly weak
377 under the baseflow conditions ($R^2 = 0.33$, $P < 0.01$). Consequently, under the baseflow conditions, C_{380}
378 remained at relatively constant values (mostly < 0.1 RU) along the headwater-mangrove-sea transect, and the
379 distribution patterns of C_{380} were not significantly different from the conservative mixing line in two out of
380 three cases (Table 3). Under the baseflow conditions, on average 42% ± 4%, 46% ± 4%, and 7% ± 10% of C_{480},
381 C_{410}, and C_{380} were contributed from the mangrove forest to the Fukido River, respectively (Fig. 3, Table 3). In
382 contrast, during the typhoon event, the highest F_{max} value of all the components along the salinity gradient
383 approximately doubled, and the sampling point where the highest F_{max} was observed shifted from at the middle
384 of the mangrove forest to the upper end of the forest (Fig. 3, Table 1), which was consistent with the distribution

of the DOM concentrations. During the typhoon event, 37% ± 6%, 42% ± 6%, and 44% ± 11% of C_{480}, C_{410}, and C_{380} were contributed from the mangrove forest to the Fukido River, respectively (Fig. 3, Table 3). The contribution of the mangrove forest to C_{380} was significantly higher during the typhoon event than under the baseflow conditions ($P < 0.05$).

Relative abundances of each PARAFAC component for each sample EEM (%F_{max}) were calculated to investigate changes in its overall importance (Fig. 3). Under the baseflow conditions, %C_{480} and %C_{410} slightly increased while %C_{380} decreased until S = ~10, reflecting inputs of C_{480} and C_{410} within the mangrove forest. In contrast, at higher salinity regions, %C_{480} and %C_{410} monotonically decreased while %C_{380} increased with salinity, suggesting the dominance of C_{380} in seawater. These results clearly show that general compositions of fluorescent DOM changed along the salinity gradient. Changes in the relative abundance of the components with salinity during the typhoon event were somewhat more variable than under the baseflow conditions, though a similar increasing pattern in %C_{380} was observed with increasing salinity.

4 Discussion

4.1 DOM composition and distribution in the Fukido River

The behavior of riverine DOM during estuarine mixing has mainly been studied in the context of changes in DOC concentration along salinity gradients. The dynamics of DOM in wetland-influenced coastal rivers can be more complex than the simple mixing of riverine DOM with seawater because of additional DOM supply from wetlands (Cawley et al., 2014; Dittmar et al., 2006; Maie et al., 2012). If we assumed a simple two-endmember mixing model for the DOM fractions and PARAFAC components, all data should be on a straight line (conservative mixing line) connecting headwater and seawater data points. However, the positive deviations of the quantitative parameters along the salinity gradient in Figure 3 indicate significant non-conservative mixing in most cases (Table 3). Although seagrasses and aquatic macrophytes and macroalgae have been suggested as a source of DOM to mangrove rivers (Maie et al., 2012, 2006, 2005), they were not observed within the Fukido mangrove forest, suggesting that the mangroves were the major additional source of DOM to the Fukido River. The increase in the HPO concentrations at S = 5–15 under the baseflow conditions indicates that precipitation

411 (or flocculation) of HPO in the river water was very small and/or the HPO inputs from the mangrove forest
412 were larger than the removal of the riverine HPO, although it is known that humic acids precipitate under the
413 interaction with cations in the seawater even at low salinity range (Sholkovitz, 1976). The HPO inputs from the
414 mangrove forest support the inputs of colored DOM from mangrove forests (Cawley et al., 2014; Dittmar et al.,
415 2006; Maie et al., 2012). We presumed that the HPO supplied from the mangrove forest was dominantly
416 composed of fulvic acids. For example, Fox (1983) reported that, in seven coastal plain estuaries located in the
417 mid-Atlantic US, humic acids were 100% removed during estuarine mixing. In contrast, fulvic acids hardly
418 precipitate (<10%) even in the seawater (Kida et al., 2016). In any case, the supplies of both HPO and HPI with
419 different biogeochemical and ecological roles from the mangrove forest support its importance as a
420 heterogeneous DOM source (Cawley et al., 2014; Dittmar et al., 2006, 2001; Maie et al., 2012). The HPO/HPI
421 fractionation reported here was quantitative, i.e., 100% of DOM was tracked in terms of carbon, in contrast to
422 colored or fluorescent DOM, which represents only a fraction of the total DOC pool. Future studies are
423 encouraged to link DOM composition and primary productivity and/or heterotrophic activity to separately
424 assess the impact of HPO and HPI on coastal ecosystems.

425 %HPO and $SUVA_{254}$ decreased, while BIX and $S_{275–295}$ increased along the headwater–mangrove–sea
426 transect (Fig. 4). These changes are highly likely to represent the general trend in the Fukido River, since they
427 were observed irrespective of sampling day (baseflow/rainy) even when the DOM concentrations and
428 compositions varied. These changes along the salinity gradient indicate the shift in DOM origin from
429 soil/terrestrial (allochthonous) to aquatic production (autochthonous) or photodegraded allochthonous DOM
430 (Helms et al., 2014, 2013). Although similar changes in $SUVA_{254}$ and BIX are often observed in estuaries
431 (Huguet et al., 2009), past literature did not conduct HPO/HPI fractionation. Therefore, the current study is the
432 first, to our knowledge, to elucidate the changes in DOM optical properties in the mangrove settings based on
433 the changes in %HPO. Until approximately $S = 25$, %HPO was >50%, $SUVA_{254}$ was >3 L mg C^{-1} m^{-1}, $S_{275–295}$
434 was <0.016 nm^{-1}, and BIX was <0.7, indicating that the dominant origins of DOM were terrestrial/mangrove
435 SOM. As reported in other studies (Butman et al., 2012; Hanley et al., 2013; Spencer et al., 2012), all of the
436 indices ($SUVA_{254}$, BIX, and $S_{275–295}$) had a significant ($P < 0.001$) moderate correlation with %HPO (Fig. S3).

Since the relationships between DOM composition and optical index values can vary from site to site (Hanley et al., 2013), establishing their relationships in a given site of interest is required. As current mangrove river studies are mostly conducted in mangrove forests with peaty soils (Cawley et al., 2014; Dittmar et al., 2006, 2001; Maie et al., 2012), the results in this study can serve as a basis for the relationships between the DOM composition and studied optical indices in rivers that flow on mineral mangrove soils in the subtropical climate. The unexplained variation of %HPO values by the optical indices in Fig. S3 indicate the limited potential of these indices to predict %HPO values in this mangrove area, which may be due to the small number of samples and the complex nature of the mangrove biogeochemistry.

The PARAFAC analysis of fluorescence EEMs provided further evidence that the mangrove forest functioned as a major contributor of heterogeneous DOM to the Fukido River (Fig. 3, Table 3). The most dominant fluorescence component in the Fukido River was C_{480}, which was reported to ubiquitously exist in a range of environments, including mangrove rivers and salt marshes (Maie et al., 2014; Osburn et al., 2016; Yamashita et al., 2010). A similar PARAFAC component was reported as a dominant component in humic and fulvic acid fractions in estuarine soils and sediments (Santín et al., 2009). Other than humic substances derived from the mangrove soil, mangrove leaf-derived lignin and tannins that underwent oxidative decompositions and polycondensation reactions could be a major source of C_{480} (Maie et al., 2008, 2007). A recent study found a strong relationship between F_{max} values of C_{480} and lignin concentrations and proposed C_{480} as a terrestrial DOM marker (Osburn et al., 2016). The other humic-like component C_{410} has been recognized as ubiquitous in the environment and also reported to be dominant in humic fractions in estuarine soils and sediments (Santín et al., 2009). In the Fukido River, the F_{max} values of C_{480} and C_{410} correlated very well ($R^2 = 0.99$, $P < 0.001$), strongly suggesting that they were derived from the same source and controlled by common environmental processes. Considering that C_{480} and C_{410} existed at high levels both at the headwater and within the mangrove forest, but at low levels in the seawater, they were most likely derived from the catchment and mangrove soil. Photodegradation is a well-known process that decreases red-shifted humic-like fluorescence (Helms et al., 2013). Thus, the low levels of C_{480} and C_{410} fluorescence in seawater samples could result from extensive

photodegradation of the terrestrially- and mangrove-derived humic-like fluorescence components, as well as the source difference.

In contrast to C_{480} and C_{410}, no systematic changes in Fmax values of C_{380} were observed along the salinity gradient under the baseflow conditions (Fig. 3, Table 3). The fluorescence property of C_{380} could be a combination of protein-like fluorescence and UV-C humic fluorescence. Fluorescence components responsible for these fluorescence were considered photo-refractory because of the blue-shifted excitation maximum (Murphy et al., 2018; Stedmon and Markager, 2005b). The rapid attenuation of UV-B light in the water column would restrict the photodegradation of these components to a thin layer at the surface (Stedmon and Markager, 2005b), even though UV-C humic-like fluorescence is intrinsically susceptible to photodegradation (Boehme and Coble, 2000). Thus, it is not surprising that C_{380} was observed at higher relative abundance at the seawater sampling point. Other than proteins, tannins derived from mangrove litter are known to fluoresce in the protein fluorescence region (Maie et al., 2008, 2007). Therefore, there were three possible origins of C_{380} in this study, which were humic substances exported from the catchment and mangrove soil, tannins leached from mangrove litter, and autochthonous production of proteinaceous materials (Stedmon and Markager, 2005b). Because there was no significant import of C_{380} from the mangrove forest under the baseflow conditions (Table 3), it was suggested that C_{380} was likely composed of soil humic substances and proteinaceous materials under the baseflow conditions, with an increasing proportion of proteinaceous materials with increasing salinity (Cawley et al., 2014; Maie et al., 2014; Yamashita et al., 2015, 2010). During the typhoon event, inputs of UV-C humic-like substances from the mangrove soil by dissolution of SOM may have occurred (Kida et al., 2017), because the significant import of C_{380} from the mangrove forest was observed (Fig. 3, Table 3).

It is also possible that the contribution from tannins increased during the typhoon event. It has been reported that the mangrove-derived DOM inputs to the surface water increased during a rain event via stemflow and throughfall from the mangrove forest canopy (Twilley, 1985). In addition, we found an exceptionally large amount of litter on the forest floor and river bed after the typhoon, a part of which was quantitatively measured using litter traps (Fig. 8 of Ohtsuka et al., 2019). Leaching of DOM (tannins and possibly other components)

from the mangrove litter and canopy could partly explain the increase in C_{380} levels and the shifts in optical index values (Fig. 4) during the typhoon event.

4.2 Changes in DOM composition and dynamics in the Fukido River by rainfall

A sharp, spike-like increase in the DOM concentration and the PARAFAC component levels was observed at the sampling point at the upper end of the mangrove forest during the typhoon event (Fig. 3). Several possibilities could be considered as a cause of this, such as elevated DOM supplies by surface water runoff and dissolution of SOM because of the decline in salinity due to the heavy rain followed by advective groundwater exchanges. The first possibility was considered unlikely or little, if any, since during the typhoon event, the distribution patterns of DOM along the salinity gradient was not conservative (Fig. 3) and the increase in DOC concentrations was more pronounced within the mangrove forest than at the headwater (Table 1), indicating additional DOM inputs from the mangrove soil (including groundwater) were primarily responsible for the increase in DOC concentrations and change in composition within the mangrove forest. We note that, even though we did not observe a large increase in DOC concentrations at the headwater, this did not necessarily mean that DOC flux supplied from the catchment remained unchanged. In addition, it is likely that we missed an initial pulsing of heavy rain that often is the most important for DOM export from the terrestrial landscape (Spencer et al., 2008). On the first day of the typhoon event (23 August 2015), a precipitation event of 241 mm was observed, which was considerably higher than that after the typhoon passed (14–54 mm on 24–26 August 2015). High surface water runoff and leaching of surface litter and soil layers in the catchment during the initial pulsing of the heavy rain could export a large amount of DOM to the Fukido River (Spencer et al., 2008). Indeed, we observed flooded tributaries that were turbid due to the heavy rain, which were distinctly different under the baseflow conditions. However, since we did not collect water discharge data, we discuss the cause of the increase in the DOC concentration and the PARAFAC component levels during the typhoon event.

Another possibility is that dissolution of SOM occurred because of the decline in salinity due to the heavy rain and more DOC was eventually supplied to the Fukido River by advective groundwater exchanges. Among the advective DOM dynamics in mangrove forests described elsewhere (Santos et al., 2012), terrestrial

hydraulic gradients, tidal pumping, and mangrove pumping were considered to be mainly responsible for the advective groundwater exchanges during the storm event. This second possibility (advective exchanges of increased-DOC groundwater resulting from dissolution of SOM) has been recently suggested by our laboratory model experiment using the Fukido mangrove soil (Kida et al., 2017). We demonstrated that sequential washing with freshwater (and the corresponding decline in salinity) caused dissolution of SOM from the mangrove soil, but sequential washing with artificial seawater did not. This implies that if sedimentary salinity decreases sufficiently to cause SOM dissolution, DOM can be exported by the advective exchanges at a higher level than usual. The observation in the current study may indicate that SOM accumulated by salinity-induced aggregation was re-mobilized by the increased freshwater input. Such an episodic mobilization of SOM may be limited to where the relative contribution of freshwater is high, such as the upper end of the mangrove forest and the river bed and bank. To investigate whether the decline in salinity due to the storm event occurred where there was a less freshwater influence, we monitored groundwater salinity just after the typhoon event at a place closer to the sea than on 8 March 2016 (Fig. 1). Figure S4b shows that groundwater salinity was considerably lower at first and then gradually increased to reach stable ranges that were similar to, but still lower than, those measured on 8 March 2016 under the baseflow condition (mean S = 28.1, Fig. S4a). This suggests that groundwater salinity decreased by the typhoon and still maintained low values a few days after the typhoon passed. During the typhoon event, the groundwater salinity could have been even lower. Comparing a depth trend in salinity in Figs. S4a and S4b, we noticed that deeper layers tended to have lower salinity after the typhoon event, which was contrary to the depth trend under the baseflow condition (the deeper, the higher salinity). This suggested that groundwater salinity up to ~1 m depth decreased during the typhoon event, further strengthening our hypothesis that the typhoon event decreased groundwater salinity. This decrease in salinity could be a driver of SOM dissolution and supply higher concentrations of DOM to the Fukido River. Thus, the aggregation–dissolution properties of SOM due to changes in salinity may be a key mechanism that influences DOM dynamics in mangrove forests, by enhancing advective DOM exchanges. It is currently unknown if DOM exported via SOM dissolution can be transported over long distances or undergoes re-aggregation upon encountering seawater. However, frequently reported increases in both DOM and turbidity during the rainy

539 season and rainfall events (Dittmar and Lara, 2001; Ray et al., 2018; Twilley, 1985) may indicate that a part of
540 DOM transforms into the particulate phase, although the increase in turbidity is often interpreted as a result of
541 the increase in particulate materials from the catchment and mangrove soils.
542
543 **4.3 Implications for organic matter dynamics of mangrove forest**
544 The controls on DOM dynamics by aggregation–dissolution properties discussed here are relevant to research
545 areas other than mangrove forests such as (i) widespread browning of the surface waters across northern
546 countries and (ii) reduction of DOM export from coastal freshwater wetlands due to saltwater incursion. (i)
547 Increases in DOM concentrations have been observed in freshwater across large areas of Europe and North
548 America. Among several mechanisms that explain the increase, decline in acidity and ionic strength of soil
549 solutions due to a decline in anthropogenic sulfur and sea salt deposition have been proposed as a chemical
550 mechanism (Evans et al., 2006). Increased pH and lowered ionic strength enhance dissolution of SOM, leading
551 to the increase in DOM concentration (Evans et al., 2006). (ii) As a result of global sea level rise (Church and
552 White, 2011), freshwater wetlands are suffering seawater incursion. For example, Ardón et al. (2016) reported
553 that saltwater incursion and drought together reduced DOM export from a freshwater wetland in North Carolina
554 to the estuary by 70%. They further disentangled the combined effect of salinity and drought based on an intact
555 soil column experiment and estimated that salinity decreased DOM concentration by 29% because of stimulated
556 aggregation of DOM. This was caused by only a slight increase in salinity (up to 6 ppt), indicating a highly
557 sensitive aggregation property of DOM upon salinization. Since mangrove forests are a highly variable
558 environment in terms of salinity because of their complex hydrology (from daily change by tide to seasonal
559 change by dry vs rainy season), the aggregation–dissolution properties of SOM are highly important in
560 determining magnitude of DOM outwelling and possibly SOM accumulation rate, particularly at the mixing
561 zone. The immobilization of SOM by aggregation due to high salinity (Kida et al., 2017) and the possibility of
562 dissolution of SOM due to the decline in salinity warrant the need to investigate C dynamics in mangrove forests
563 with the aggregation–dissolution properties of SOM in mind to better understand elemental cycling in mangrove
564 forests.

Our data suggest that large precipitation events can strongly influence C dynamics (Fig. 3). Most mangrove forests are located in tropical regions and are frequently struck by typhoons or hurricanes, which causes an episodic decline in salinity. In regions with clear dry and rainy seasons, mangrove forests experience a seasonal fluctuation in salinity. For example, Pérez et al. (2017) showed lower SOM and chlorophyll-a contents in the subtidal sediments during the rainy season than during the dry season in a Peruvian mangrove forest. They attributed this decrease in SOM to enhanced transport of SOM to the estuary because of increased water flow during the rainy season. We would additionally consider a decline in river-and groundwater salinity due to the increased freshwater input as an important cause of mobilization/dissolution of SOM. Similarly, in a Trat mangrove forest in Eastern Thailand, groundwater salinity up to ~2 m depth throughout the entire forest is completely fresh during the rainy season at least for 3 months because of increased river water flux, while during the dry season the groundwater is saline (Poungparn S., pers. comm.). This seasonal change in groundwater salinity could have great impacts on both SOM sequestration and DOM dynamics. Mangrove-derived DOM has been suggested to be transported over long distances to coastal and offshore waters (Dittmar et al., 2006, 2001). Because mangrove-derived DOM had more aromatic, light absorbing properties than coastal DOM (Figs. 3, 4), exported DOM would effectively attenuate both solar UV and photosynthetically active radiation, therefore directly influencing coastal primary productivity on a regional scale. Photodegradation of mangrove-derived DOM in the open coastal area would also stimulate bacterial metabolism (Tranvik, 1992).

Overall, the contribution of the Fukido mangrove forest to the DOM concentration was estimated at up to 46% of DOM and 58% of the PARAFAC components (Table 3). These results highlight the importance of the mangrove forest-derived DOM (both HPO and HPI) to the coastal ocean. We proposed that the typhoon event caused enhanced leaching of DOM from mangrove litter and dissolution of mangrove SOM, which was otherwise retained in the mangrove soil by salinity-induced aggregation (Kida et al., 2017). The aggregation–dissolution properties of SOM are crucial in determining the magnitude of DOM outwelling and expected to influence SOM accumulation rate. Future studies should elucidate underlying mechanisms that control the release of DOM with changing salinity, such as organo-mineral complexation. Increasing episodic freshwater inputs by typhoons or hurricanes would lead to an enhanced export of mangrove-derived DOM by advective

exchanges of increased-DOC groundwater resulting from dissolution of SOM. Tidal hydrology and coastal morphology should be important in influencing material cycling of mangrove forests as well as mangrove carbon storage (Twilley et al., 2018). These characteristics affect not only biogeochemical conditions in mangrove forests but also dominant mangrove species and their growth rates and microbial activity, influencing SOM accumulation and turnover rates. Therefore, it is necessary to evaluate the size of the C pool and outwelling of DOM and consequently the ecosystem services after classifying mangrove forests using the hydrological regime as a parameter.

Declarations of interest: none

Contributions: M. K., M. Tanabe, M. Tomotsune, and N.F. collected the samples with the help of other authors. M. Tanabe and M.K. conducted experiments. M. K. wrote the draft. All authors contributed to the design of the study and have reviewed and approved the final article.

Acknowledgments

We are grateful to two anonymous reviewers for detailed and constructive comments on the original manuscript. This study was supported by JSPS KAKENHI Grant Number JP15H05240 and Grant-in-Aid for JSPS Research Fellow (17J00808).

References

Alongi, D.M., 2014. Carbon cycling and storage in mangrove forests. Ann. Rev. Mar. Sci. 6, 195–219. https://doi.org/10.1146/annurev-marine-010213-135020

Ardón, M., Helton, A.M., Bernhardt, E.S., 2016. Drought and saltwater incursion synergistically reduce dissolved organic carbon export from coastal freshwater wetlands. Biogeochemistry 127, 411–426. https://doi.org/10.1007/s10533-016-0189-5

Benner, R., Weliky, K., Hedges, J.I., 1990. Early diagenesis of mangrove leaves in a tropical estuary:

Molecular-level analyses of neutral sugars and lignin-derived phenols. Geochim. Cosmochim. Acta 54, 1991–2001. https://doi.org/10.1016/0016-7037(90)90267-O

Blazevic, A., Orlowska, E., Kandioller, W., Jirsa, F., Keppler, B.K., Tafili-Kryeziu, M., Linert, W., Krachler, R.F., Krachler, R., Rompel, A., 2016. Photoreduction of Terrigenous Fe-Humic Substances Leads to Bioavailable Iron in Oceans. Angew. Chemie Int. Ed. 55, 6417–6422. https://doi.org/10.1002/anie.201600852

Boehme, J.R., Coble, P.G., 2000. Characterization of colored dissolved organic matter using high-energy laser fragmentation. Environ. Sci. Technol. 34, 3283–3290. https://doi.org/10.1021/es9911263

Bricaud, A., Morel, A., Prieur, L., 1981. Absorption by dissolved organic matter of the sea (yellow substance) in the UV and visible domains. Limnol. Oceanogr. 26, 43–53. https://doi.org/10.4319/lo.1981.26.1.0043

Butman, D., Raymond, P.A., Butler, K., Aiken, G., 2012. Relationships between Δ 14 C and the molecular quality of dissolved organic carbon in rivers draining to the coast from the conterminous United States. Global Biogeochem. Cycles 26, 1–15. https://doi.org/10.1029/2012GB004361

Cawley, K.M., Ding, Y., Fourqurean, J., Jaffé, R., 2012. Characterising the sources and fate of dissolved organic matter in Shark Bay, Australia: a preliminary study using optical properties and stable carbon isotopes. Mar. Freshw. Res. 63, 1098. https://doi.org/10.1071/MF12028

Cawley, K.M., Yamashita, Y., Maie, N., Jaffé, R., 2014. Using optical properties to quantify fringe mangrove inputs to the dissolved organic matter (DOM) pool in a subtropical estuary. Estuaries and Coasts 37, 399–410. https://doi.org/10.1007/s12237-013-9681-5

Church, J.A., White, N.J., 2011. Sea-level rise from the late 19th to the early 21st century. Surv. Geophys. 32, 585–602. https://doi.org/10.1007/s10712-011-9119-1

Dittmar, T., Hertkorn, N., Kattner, G., Lara, R.J., 2006. Mangroves, a major source of dissolved organic carbon to the oceans. Global Biogeochem. Cycles 20, 7p. https://doi.org/10.1029/2005GB002570

Dittmar, T., Lara, R.J., 2001. Driving forces behind nutrient and organic matter dynamics in a mangrove tidal creek in North Brazil. Estuar. Coast. Shelf Sci. 52, 249–259. https://doi.org/10.1006/ecss.2000.0743

Dittmar, T., Lara, R.J., Kattner, G., 2001. River or mangrove? Tracing major organic matter sources in

tropical Brazilian coastal waters. Mar. Chem. 73, 253–271. https://doi.org/10.1016/S0304-4203(00)00110-9

Evans, C.D., Chapman, P.J., Clark, J.M., Monteith, D.T., Cresser, M.S., 2006. Alternative explanations for rising dissolved organic carbon export from organic soils. Glob. Chang. Biol. 12, 2044–2053. https://doi.org/10.1111/j.1365-2486.2006.01241.x

Fichot, G., Benner, R., 2012. The spectral slope coefficient of chromophoric dissolved organic matter (S 275 – 295) as a tracer of terrigenous dissolved organic carbon in river-influenced ocean margins 57, 1453–1466. https://doi.org/10.4319/lo.2012.57.5.1453

Fox, L.E., 1983. The removal of dissolved humic acid during estuarine mixing. Estuar. Coast. Shelf Sci. 16, 431–440. https://doi.org/10.1016/0272-7714(83)90104-X

Gledhill, M., Buck, K.N., 2012. The organic complexation of iron in the marine environment: a review. Front. Microbiol. 3, 1–17. https://doi.org/10.3389/fmicb.2012.00069

Hanley, K.W., Wollheim, W.M., Salisbury, J., Huntington, T., Aiken, G., 2013. Controls on dissolved organic carbon quantity and chemical character in temperate rivers of North America. Global Biogeochem. Cycles 27, 492–504. https://doi.org/10.1002/gbc.20044

Helms, J.R., Mao, J., Stubbins, A., Schmidt-Rohr, K., Spencer, R.G.M., Hernes, P.J., Mopper, K., 2014. Loss of optical and molecular indicators of terrigenous dissolved organic matter during long-term photobleaching. Aquat. Sci. 76, 353–373. https://doi.org/10.1007/s00027-014-0340-0

Helms, J.R., Stubbins, A., Perdue, E.M., Green, N.W., Chen, H., Mopper, K., 2013. Photochemical bleaching of oceanic dissolved organic matter and its effect on absorption spectral slope and fluorescence. Mar. Chem. 155, 81–91. https://doi.org/10.1016/j.marchem.2013.05.015

Helms, J.R., Stubbins, A., Ritchie, J.D., Minor, E.C., Kieber, D.J., Mopper, K., 2008. Absorption spectral slopes and slope ratios as indicators of molecular weight, source, and photobleaching of chromophoric dissolved organic matter. Limnol. Oceanogr. 53, 955–969. https://doi.org/10.4319/lo.2008.53.3.0955

Hu, C., Muller-Karger, F.E., Zepp, R.G., 2002. Absorbance, absorption coefficient, and apparent quantum yield: A comment on common ambiguity in the use of these optical concepts. Limnol. Oceanogr. 47,

1261–1267. https://doi.org/10.4319/lo.2002.47.4.1261

Huguet, A., Vacher, L., Relexans, S., Saubusse, S., Froidefond, J.M., Parlanti, E., 2009. Properties of fluorescent dissolved organic matter in the Gironde Estuary. Org. Geochem. 40, 706–719. https://doi.org/10.1016/j.orggeochem.2009.03.002

Imai, A., Fukushima, T., Matsushige, K., Kim, Y.H., 2001. Fractionation and characterization of dissolved organic matter in a shallow eutrophic lake, its inflowing rivers, and other organic matter sources. Water Res. 35, 4019–4028. https://doi.org/10.1016/S0043-1354(01)00139-7

Kida, M., Ohtsuka, T., Kato, T., Suzuki, T., Fujitake, N., 2016. Evaluation of salinity effect on quantitative analysis of aquatic humic substances using nonionic DAX-8 resin. Chemosphere 146, 129–132. https://doi.org/10.1016/j.chemosphere.2015.12.031

Kida, M., Tomotsune, M., Iimura, Y., Kinjo, K., Ohtsuka, T., Fujitake, N., 2017. High salinity leads to accumulation of soil organic carbon in mangrove soil. Chemosphere 177, 51–55. https://doi.org/10.1016/j.chemosphere.2017.02.074

Kothawala, D.N., Murphy, K.R., Stedmon, C.A., Weyhenmeyer, G.A., Tranvik, L.J., 2013. Inner filter correction of dissolved organic matter fluorescence. Limnol. Oceanogr. Methods 11, 616–630. https://doi.org/10.4319/lom.2013.11.616

Kristensen, E., Bouillon, S., Dittmar, T., Marchand, C., 2008. Organic carbon dynamics in mangrove ecosystems: A review. Aquat. Bot. 89, 201–219. https://doi.org/10.1016/j.aquabot.2007.12.005

Lee, S.Y., 1995. Mangrove outwelling: a review. Hydrobiologia 295, 203–212. https://doi.org/10.1007/BF00029127

Maher, D.T., Santos, I.R., Golsby-Smith, L., Gleeson, J., Eyre, B.D., 2013. Groundwater-derived dissolved inorganic and organic carbon exports from a mangrove tidal creek: The missing mangrove carbon sink? Limnol. Oceanogr. 58, 475–488. https://doi.org/10.4319/lo.2013.58.2.0475

Maie, N., Parish, K.J., Watanabe, A., Knicker, H., Benner, R., Abe, T., Kaiser, K., Jaffé, R., 2006. Chemical characteristics of dissolved organic nitrogen in an oligotrophic subtropical coastal ecosystem. Geochim. Cosmochim. Acta 70, 4491–4506. https://doi.org/10.1016/j.gca.2006.06.1554

Maie, N., Pisani, O., Jaffé, R., 2008. Mangrove tannins in aquatic ecosystems: Their fate and possible influence on dissolved organic carbon and nitrogen cycling. Limnol. Oceanogr. 53, 160–171.

Maie, N., Scully, N.M., Pisani, O., Jaffé, R., 2007. Composition of a protein-like fluorophore of dissolved organic matter in coastal wetland and estuarine ecosystems. Water Res. 41, 563–570. https://doi.org/10.1016/j.watres.2006.11.006

Maie, N., Sekiguchi, S., Watanabe, A., Tsutsuki, K., Yamashita, Y., Melling, L., Cawley, K.M., Shima, E., Jaffé, R., 2014. Dissolved organic matter dynamics in the oligo/meso-haline zone of wetland-influenced coastal rivers. J. Sea Res. 91, 58–69. https://doi.org/10.1016/j.seares.2014.02.016

Maie, N., Yamashita, Y., Cory, R.M., Boyer, J.N., Jaffé, R., 2012. Application of excitation emission matrix fluorescence monitoring in the assessment of spatial and seasonal drivers of dissolved organic matter composition: Sources and physical disturbance controls. Appl. Geochemistry 27, 917–929. https://doi.org/10.1016/j.apgeochem.2011.12.021

Maie, N., Yang, C., Parish, K., Jaffe, R., 2005. Chemical characteristics of dissolved organic matter in an oligotrophic subtropical wetland / estuarine ecosystem 50, 23–35.

McKnight, D.M., Boyer, E.W., Westerhoff, P.K., Doran, P.T., Kulbe, T., Andersen, D.T., 2001. Spectrofluorometric characterization of dissolved organic matter for indication of precursor organic material and aromaticity. Limnol. Oceanogr. 46, 38–48. https://doi.org/10.4319/lo.2001.46.1.0038

Murphy, K.R., 2011. A note on determining the extent of the water Raman peak in fluorescence spectroscopy. Appl. Spectrosc. 65, 233–236. https://doi.org/10.1366/10-06136

Murphy, K.R., Hambly, A., Singh, S., Henderson, R.K., Baker, A., Stuetz, R., Khan, S.J., 2011. Organic matter fluorescence in municipal water recycling schemes: Toward a unified PARAFAC model. Environ. Sci. Technol. 45, 2909–2916. https://doi.org/10.1021/es103015e

Murphy, K.R., Stedmon, C.A., Graeber, D., Bro, R., 2013. Fluorescence spectroscopy and multi-way techniques. PARAFAC. Anal. Methods 5, 6557–6566. https://doi.org/10.1039/c3ay41160e

Murphy, K.R., Stedmon, C.A., Wenig, P., Bro, R., 2014. OpenFluor- an online spectral library of auto-fluorescence by organic compounds in the environment. Anal. Methods 6, 658–661.

https://doi.org/10.1039/c3ay41935e

Murphy, K.R., Timko, S.A., Gonsior, M., Powers, L.C., Wünsch, U.J., Stedmon, C.A., 2018. Photochemistry illuminates ubiquitous organic matter fluorescence spectra. Environ. Sci. Technol. 52, 11243–11250. https://doi.org/10.1021/acs.est.8b02648

Odum, W.E., 1968. A research challenge: evaluating the productivity of coastal and estuarine water. Proc. Second Sea Grant Conf. 63–64.

Ohtsuka, T., Tomotsune, M., Suchewaboripont, V., Iimura, Y., Kida, M., Yoshitake, S., Kondo, M., Kinjo, K., 2019. Stand dynamics and aboveground net primary productivity of a mature subtropical mangrove forest on Ishigaki Island, south-western Japan. Reg. Stud. Mar. Sci. 100516. https://doi.org/10.1016/j.rsma.2019.100516

Osburn, C.L., Boyd, T.J., Montgomery, M.T., Bianchi, T.S., Coffin, R.B., Paerl, H.W., 2016. Optical proxies for terrestrial dissolved organic matter in estuaries and coastal waters. Front. Mar. Sci. 2. https://doi.org/10.3389/fmars.2015.00127

Pérez, A., Gutiérrez, D., Saldarriaga, M.S., Sanders, C.J., 2017. Hydrological controls on the biogeochemical dynamics in a Peruvian mangrove forest. Hydrobiologia 803, 69–86. https://doi.org/10.1007/s10750-017-3118-2

Ray, R., Baum, A., Rixen, T., Gleixner, G., Jana, T.K., 2018. Exportation of dissolved (inorganic and organic) and particulate carbon from mangroves and its implication to the carbon budget in the Indian Sundarbans. Sci. Total Environ. 621, 535–547. https://doi.org/10.1016/j.scitotenv.2017.11.225

Santín, C., Yamashita, Y., Otero, X.L., Álvarez, M.Á., Jaffé, R., 2009. Characterizing humic substances from estuarine soils and sediments by excitation-emission matrix spectroscopy and parallel factor analysis. Biogeochemistry 96, 131–147. https://doi.org/10.1007/s10533-009-9349-1

Santos, I.R., Eyre, B.D., Huettel, M., 2012. The driving forces of porewater and groundwater flow in permeable coastal sediments: A review. Estuar. Coast. Shelf Sci. 98, 1–15. https://doi.org/10.1016/j.ecss.2011.10.024

Sholkovitz, E.R., 1976. Flocculation of dissolved organic and inorganic matter during the mixing of river

water and seawater. Geochim. Cosmochim. Acta 40, 831–845. https://doi.org/10.1016/0016-7037(76)90035-1

Soto Cárdenas, C., Gerea, M., Garcia, P.E., Pérez, G.L., Diéguez, M.C., Rapacioli, R., Reissig, M., Queimaliños, C., 2017. Interplay between climate and hydrogeomorphic features and their effect on the seasonal variation of dissolved organic matter in shallow temperate lakes of the Southern Andes (Patagonia, Argentina): a field study based on optical properties. Ecohydrology 10, e1872. https://doi.org/10.1002/eco.1872

Spencer, R.G., Butler, K.D., Aiken, G.R., 2012. Dissolved organic carbon and chromophoric dissolved organic matter properties of rivers in the USA. J. Geophys. Res. 117, 1–14. https://doi.org/10.1029/2011JG001928

Spencer, R.G.M., Aiken, G.R., Wickland, K.P., Striegl, R.G., Hernes, P.J., 2008. Seasonal and spatial variability in dissolved organic matter quantity and composition from the Yukon River basin, Alaska. Global Biogeochem. Cycles 22, 1–13. https://doi.org/10.1029/2008GB003231

Stedmon, C., Markager, S., 2005a. Resolving the variability in dissolved organic matter fluorescence in a temperate estuary and its catchment using PARAFAC analysis. Limnol. Oceanogr. 50, 686–697. https://doi.org/10.4319/lo.2005.50.2.0686

Stedmon, C., Markager, S., 2005b. Tracing the production and degradation of autochthonous fractions of dissolved organic matter by fluorescence analysis. Limnol. Oceanogr. 50, 1415–1426. https://doi.org/10.4319/lo.2005.50.5.1415

Stieglitz, T.C., Clark, J.F., Hancock, G.J., 2013. The mangrove pump: The tidal flushing of animal burrows in a tropical mangrove forest determined from radionuclide budgets. Geochim. Cosmochim. Acta 102, 12–22. https://doi.org/10.1016/j.gca.2012.10.033

Thurman, E.M., Malcolm, R.L., 1981. Preparative isolation of aquatic humic substances. Environ. Sci. Technol. 15, 463–466. https://doi.org/10.1021/es00086a012

Tranvik, L.J., 1992. Allochthonous dissolved organic matter as an energy source for pelagic bacteria and the concept of the microbial loop. Hydrobiologia 229, 107–114. https://doi.org/10.1007/BF00006994

Tsuda, K., Takata, A., Shirai, H., Kozaki, K., Fujitake, N., 2012. A method for quantitative analysis of aquatic humic substances in clear water based on carbon concentration. Anal. Sci. 28, 1017–1020. https://doi.org/10.2116/analsci.28.1017

Twilley, R., 1985. The exchange of organic carbon in basin mangrove forests in a southwest Florida estuary. Estuar. Coast. Shelf Sci. 20, 543–557.

Twilley, R.R., Rovai, A.S., Riul, P., 2018. Coastal morphology explains global blue carbon distributions. Front. Ecol. Environ. 1–6. https://doi.org/10.1002/fee.1937

Wafar, S., Untawale, A.G., Wafar, M., 1997. Litter fall and energy flux in a mangrove ecosystem. Estuar. Coast. Shelf Sci. 44, 111–124. https://doi.org/10.1006/ecss.1996.0152

Weishaar, J.L., Aiken, G.R., Bergamaschi, B.A., Fram, M.S., Fujii, R., Mopper, K., 2003. Evaluation of specific ultraviolet absorbance as an indicator of the chemical composition and reactivity of dissolved organic carbon. Environ. Sci. Technol. 37, 4702–4708. https://doi.org/10.1021/es030360x

Yamashita, Y., Fichot, C.G., Shen, Y., Jaffé, R., Benner, R., 2015. Linkages among fluorescent dissolved organic matter, dissolved amino acids and lignin-derived phenols in a river-influenced ocean margin. Front. Mar. Sci. 2, 1–14. https://doi.org/10.3389/fmars.2015.00092

Yamashita, Y., Scinto, L.J., Maie, N., Jaffé, R., 2010. Dissolved organic matter characteristics across a subtropical wetland's landscape: Application of optical properties in the assessment of environmental dynamics. Ecosystems 13, 1006–1019. https://doi.org/10.1007/s10021-010-9370-1

Table 1. Sampling dates, basic water chemistry, DOM concentration and composition, and its optical data

yyyy/mm/dd	Salinity	pH	DOM	%HPO	$SUVA_{254}$	$S_{275–295}$	BIX	yyyy/mm/dd	Salinity	pH	DOM	%HPO	$SUVA_{254}$	$S_{275–295}$	BIX
			mg C L^{-1}		L mg C^{-1} m^{-1}	nm^{-1}					mg C L^{-1}		L mg C^{-1} m^{-1}	nm^{-1}	
2014/9/30	0.2	7.4	0.90	68.8	4.1	0.013	ND	2015/8/25	0.2	7.8	1.61	69.6	3.3	0.013	0.60
	0.4	7.4	1.26	66.0	4.2	0.012	ND		1.6	8.2	3.21	63.1	3.4	0.015	0.68
	11.3	7.3	1.60	64.3	3.8	0.014	ND		2.4	8.1	2.29	63.4	3.4	0.013	0.66
	24.7	7.3	1.67	61.1	3.3	0.016	ND		4.0	8.1	2.32	61.3	3.4	0.014	0.62
	29.8	7.4	1.39	57.7	3.1	0.017	ND		6.1	8.0	2.11	57.6	3.2	0.014	0.69
	32.2	8.0	0.67	50.5	2.1	0.019	ND		11.4	8.0	2.07	58.9	3.0	0.014	0.66
									25.7	8.1	1.29	39.0	2.0	0.016	0.83
2014/11/21	0.2	7.3	0.99	64.8	3.6	0.012	ND	2015/8/26	0.2	8.0	1.63	68.2	3.0	-	0.68
	6.7	7.7	1.33	57.9	3.4	0.016	ND		1.0	8.3	3.71	63.1	3.8	-	0.66
	14.3	7.6	1.56	60.0	3.5	0.016	ND		1.5	8.2	2.55	65.0	3.5	-	0.72
	22.4	7.5	1.55	57.7	3.3	0.017	ND		1.8	8.2	2.42	60.5	3.3	-	0.69
	27.9	7.6	1.29	52.5	2.7	0.018	ND		2.4	8.1	2.58	64.9	3.4	-	0.68
	30.9	7.8	0.93	52.6	2.5	0.017	ND		3.1	8.0	2.38	63.2	3.3	-	0.66
									10.0	8.2	2.03	57.3	2.7	-	0.71
2015/1/23	0.2	7.2	0.86	67.9	ND	ND	ND	2015/11/10	0.2	7.2	1.00	66.6	4.1	0.012	0.67
	4.2	7.4	1.16	60.4	ND	ND	ND		10.0	7.2	2.10	62.8	3.7	0.016	0.61
	8.5	7.4	1.22	62.2	ND	ND	ND		10.4	7.4	1.63	59.1	3.6	0.015	0.61
	17.1	7.4	1.32	58.4	ND	ND	ND		17.1	7.4	1.55	55.4	3.6	0.015	0.73
	23.8	7.4	1.12	53.5	ND	ND	ND		18.0	7.4	1.32	58.6	3.3	0.015	0.68
	28.4	7.5	1.12	47.5	ND	ND	ND		26.2	7.6	1.12	54.1	3.0	0.016	0.76
	32.7	7.8	1.10	45.9	ND	ND	ND		32.7	8.2	0.79	42.3	2.1	0.012	-
2015/5/14	0.1	7.7	1.07	65.0	4.2	0.012	ND	2016/3/8	0.3	7.6	0.91	68.5	3.8	0.013	0.61
	3.0	7.8	1.54	63.6	3.8	0.013	ND		0.4	7.5	1.11	66.0	3.5	0.013	0.67
	3.8	7.8	1.54	64.3	3.8	0.013	ND		2.7	7.6	1.18	67.3	3.9	0.013	0.57
	8.2	7.9	1.64	55.8	3.8	0.014	ND		5.4	7.5	1.18	67.3	3.6	0.014	0.57
	12.9	7.7	1.34	52.2	3.8	0.015	ND		10.0	7.4	1.17	61.8	3.2	0.015	0.61
	18.7	7.8	1.32	57.1	3.3	0.015	ND		17.9	7.5	1.22	59.2	2.9	0.015	0.62
	20.2	7.9	1.21	57.7	3.0	0.014	ND		29.8	8.0	0.98	45.5	1.5	0.018	0.83
2015/8/24	0.3	7.1	1.55	71.0	3.1	-	0.55	2016/6/20	0.1	7.3	1.78	68.2	4.1	0.011	0.64
	1.7	7.6	3.20	63.0	3.6	-	0.61		0.4	7.5	0.77	56.1	3.1	0.012	0.66
	1.7	7.5	2.11	62.9	3.3	-	0.58		3.3	7.5	1.56	65.6	3.8	0.012	0.57
	3.6	7.7	2.12	60.3	3.2	-	0.62		10.6	7.4	1.56	59.8	3.5	0.014	0.57
	5.9	7.7	2.02	57.4	3.1	-	0.74		16.7	7.4	1.47	59.1	3.3	0.014	0.60
	8.4	7.9	1.90	59.8	3.0	-	0.69		23.7	7.4	1.17	54.6	3.0	0.014	0.61
	32.2	8.2	0.88	33.6	0.8	-	0.93		31.2	7.9	1.03	43.1	1.7	0.016	0.78

ND not determined

$S_{275–295}$ on 24 and 26 August 2015 was not used due to disturbance of spectra caused by auto-switching of the light source of the spectrophotometer during measurements.

DOM= dissolved organic matter, %HPO = proportion of hydrophobic fraction in DOM, $SUVA_{254}$ = specific UV absorbance at 254 nm, $S_{275–295}$ = spectral slope determined between 275 nm and 295 nm, and BIX = biological index.

Table 2. Characteristics of the three PARAFAC components derived from the Fukido River.

Component	Excitation Maximum	Emission maximum	Origin	Assignment	Reference
C_{480}	< 265 (360)	478	Terrestrial/ autochthonous	highly conjugated aromatic material resemble isolated fulvic acids from soils and sediments	Osburn et al., 2016
				ubiquitous humic-like	Stedmon and Markager., 2005a Yamashita et al., 2010
C_{410}	< 265 (325)	409	Terrestrial/ autochthonous/ anthropogenic	ubiquitous humic-like suggested as photo-labile and agricultural land use derived	Stedmon and Markager., 2005a Yamashita et al., 2010
				fulvic acid-type, suggested to be bio-available	Cawley et al., 2012
C_{380}	< 265 (275)	380	Terrestrial/ autochthonous	combination of protein-like component and UV-C humic component	
				photo-refractory or photo-producible	Murphy et al., 2018

Table 3. Contribution of the mangrove forest to DOM fractions and PARAFAC components (in percentage).

Sampling date	DOM	HPO	HPI	C_{480}	C_{410}	C_{380}
30-Sep-14	46.2	47.6*	44.1	ND	ND	ND
21-Nov-14	28.8	27.8	30.2	ND	ND	ND
23-Jan-15	16.6*	17.9	15.0*	ND	ND	ND
14-May-15	18.9	13.7	25.2*	ND	ND	ND
24-Aug-15[§]	20.5	16.8*	25.8	40.4	43.8	58.1
25-Aug-15[§]	27.1	21.5*	33.0	41.5	49.1	42.6
26-Aug-15[§]	24.2	22.2*	27.3	29.0	33.6	31.9
10-Nov-15	31.3	34.2	27.8	43.4	47.0	18.7*
8-Mar-16	17.2	20.7	12.1*	36.9	40.6	−19.4*
20-Jun-16	30.3	39.7	17.1*	47.0	49.2	20.9

* not significantly different from the conservative mixing (F-test, $P > 0.05$).

[§] typhoon event (see the main text)

Figure 1. a) Fukido mangrove forest on Ishigaki Island, Okinawa, Japan. The white solid line indicates the mangrove forest area. The dotted line indicates the Fukido River from which water samples were collected. Black dots with white circles indicate the surface water sampling points, while the black square with white frame indicates groundwater sampling point. On every sampling day, salinity continuously increased from the headwater to the sea sampling point. b) monthly average precipitation and air temperature record between 1981 and 2010.

Figure 2. Daily precipitation record and sampling timing. Arrows indicate the sampling timing with B denoting baseflow condition (any period more than 24 h after a rain event). On 24–26 August 2015, successive three-day sampling was conducted to capture the changes in dissolved organic matter concentrations and compositions caused by heavy rains due to Typhoon Goni. The precipitation on 23, 24, 25 and 26 August 2015 was 241, 33, 54 and 14 mm, respectively.

Figure 3. Dissolved organic matter (DOM) and hydrophobic and hydrophilic fraction of DOM (HPO and HPI) concentrations (upper row), F_{max} of the identified PARAFAC components (middle row), and the relative distribution of the PARAFAC components (bottom row), all plotted along salinity. The left panel shows the results under baseflow condition, while the right panel is the results during the typhoon event. Solid lines are an example of simple conservative mixing model lines connecting headwater and the sea for 20 June 2016 samples (left panel) and 24 August 2015 samples (right panel). Note the different scale of the y-axis between the left and right panels.

Figure 4. (a) proportion of hydrophobic fraction in DOM (%HPO), (b) specific UV absorbance at 254 nm ($SUVA_{254}$), (c) biological index (BIX), and (d) spectral slope determined between 275 nm and 295 nm ($S_{275–295}$) along the salinity gradient. White circles represent samples collected under the baseflow conditions, while black circles indicate samples during the typhoon event.

Figure 5. Groundwater DOC concentration at different depth collected every 2 h for 24 h on 8 March 2016. The regression line (least squares) is indicated by a solid line, where the x-intercept is 1.27 mg C L^{-1}. The first collected samples (represented by white circle) were omitted from the regression analysis due to contamination possibly from the vinyl chloride pipe and plastic syringe used for groundwater collection.

Figure 1

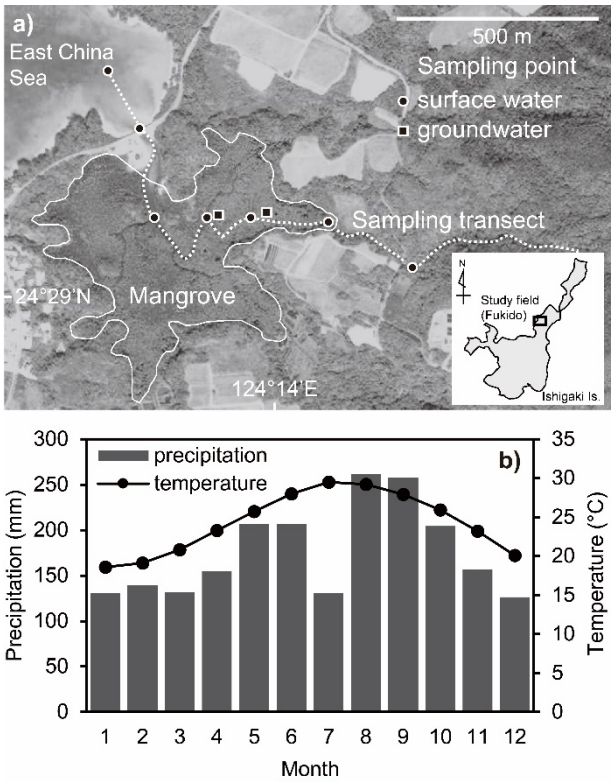

Figure 2

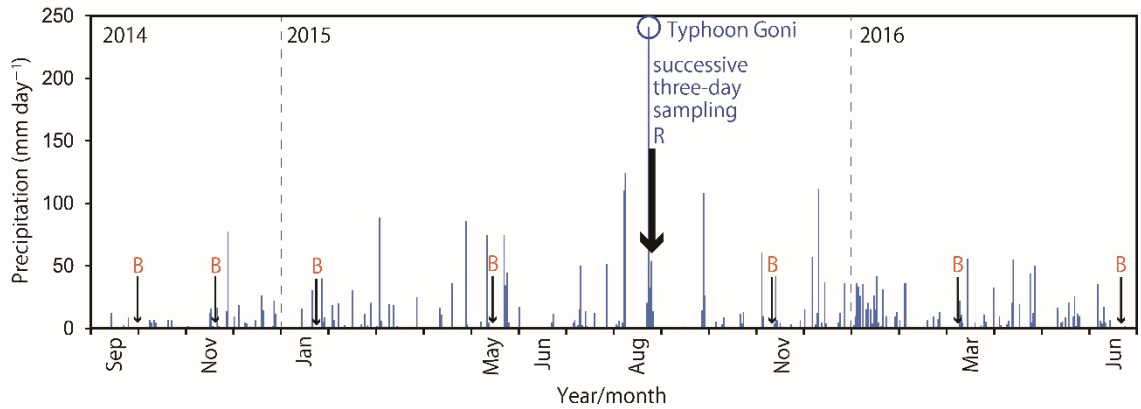

Figure 3

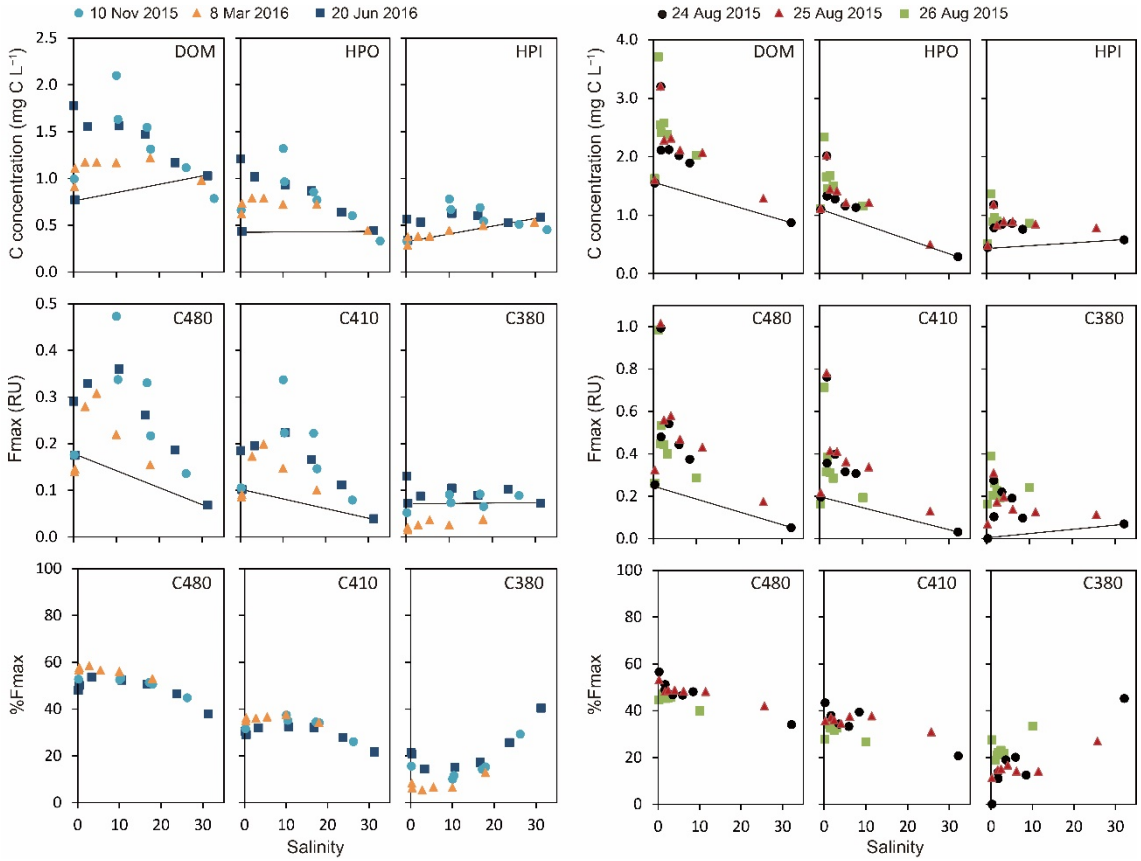
10 Nov 2015
8 Mar 2016
20 Jun 2016
24 Aug 2015
25 Aug 2015
26 Aug 2015
DOM
HPO
HPI
C480
C410
C380
C concentration (mg C L⁻¹)
Fmax (RU)
%Fmax
Salinity

Figure 4

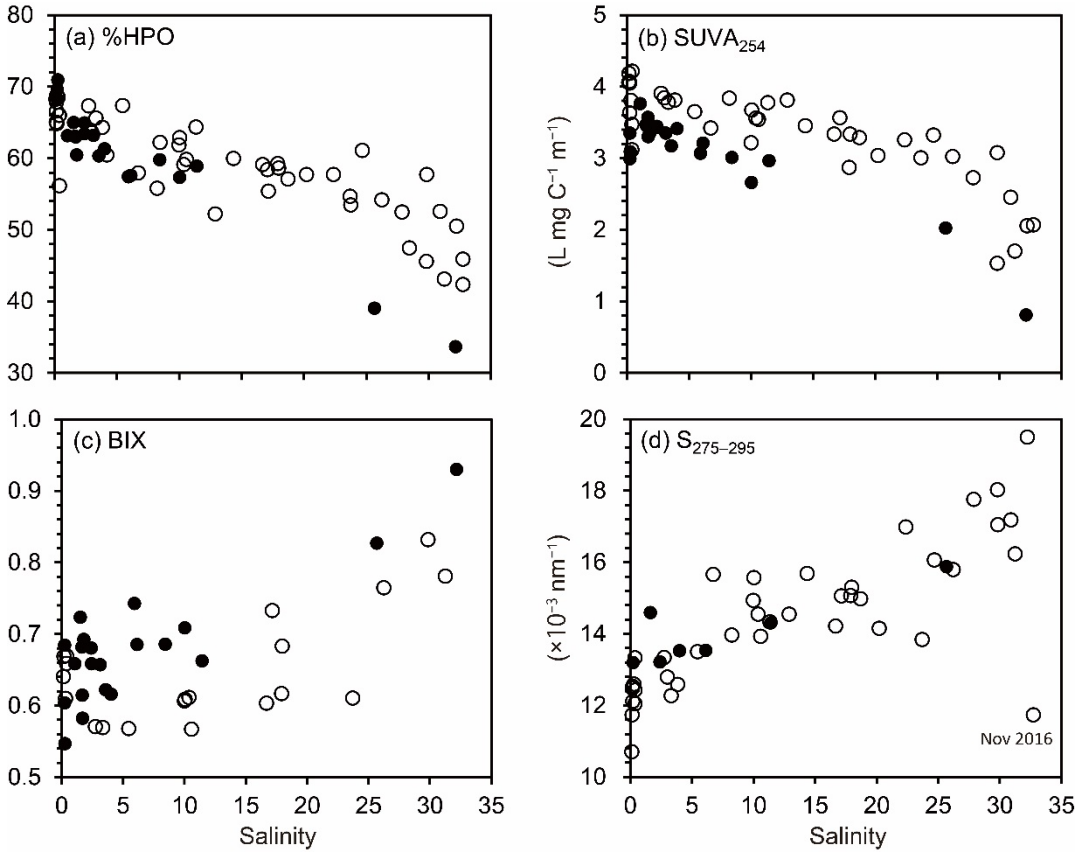

Figure 5

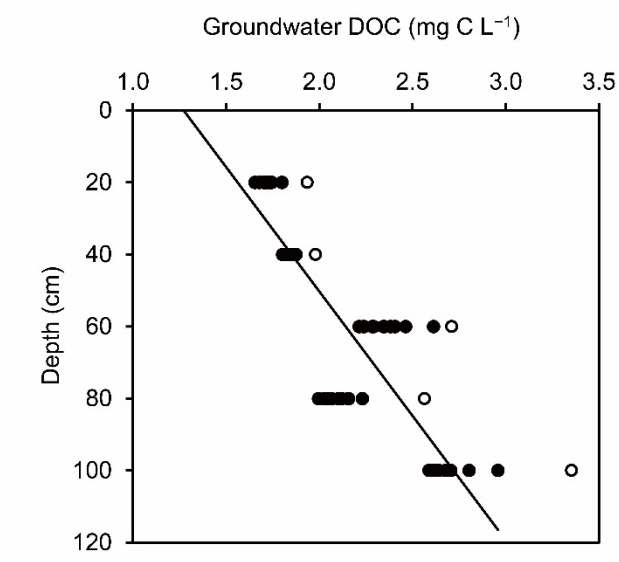

Supporting information for:

Changes in dissolved organic matter composition and dynamics in a subtropical mangrove river driven by rainfall

Journal: Estuarine, Coastal and Shelf Science

Morimaru Kida[1†‡*], Mai Tanabe[1], Mitsutoshi Tomotsune[1¶], Shinpei Yoshitake[2] Kazutoshi Kinjo[3], Toshiyuki Ohtsuka[4], and Nobuhide Fujitake[1]

1 Graduate School of Agricultural Science, Kobe University, 1 Rokkodai, Nada, Kobe, Hyogo 657-8501, Japan

†Research Fellow of Japan Society for the Promotion of Science

2 Takayama Field Station, River Basin Research Center, Gifu University, 919-47, Iwai, Takayama, Gifu 506-0815, Japan

3 Faculty of Agriculture, University of the Ryukyus, 1 Senbaru, Nishihara, Nakagami, Okinawa 903-0213, Japan

4 River Basin Research Center, Gifu University, 1-1 Yanagito, Gifu, Gifu 501-1193, Japan

‡ Present address: Research Group for Marine Geochemistry (ICBM-MPI Bridging Group), Carl von Ossietzky University of Oldenburg, Institute for Chemistry and Biology of the Marine Environment (ICBM), Carl-von-Ossietzky-Str. 9-11, 26129 Oldenburg, Germany

¶ Present address: Faculty of Education and Integrated Arts and Sciences, Waseda University, 2-2 Wakamatsu, Shinjuku, Tokyo 162–8480, Japan

*Corresponding author: Morimaru Kida

Address: marumori1004@gmail.com

Tell: 078-803-5846

ORCID ID: 0000-0002-9908-2012 (M.K.)

Content: 4 figures & 1 table

Table S1. Data of a preliminary sampling on 14 May 2013 when a heavy rain (57 mm) was observed one day before sampling.

Salinity	pH	DOM	HPO	HPI	%HPO
		(mg C L^{-1})	(mg C L^{-1})	(mg C L^{-1})	
0.1	7.4	1.41	1.07	0.34	75.9
0.5	7.5	1.48	1.05	0.42	71.5
1.8	7.6	1.48	1.01	0.47	68.5
3.2	7.6	1.46	0.96	0.50	65.5
5.3	7.6	1.52	0.95	0.56	63.0
8.9	7.6	1.22	0.75	0.48	61.1
27.7	8.1	0.92	0.44	0.49	47.5

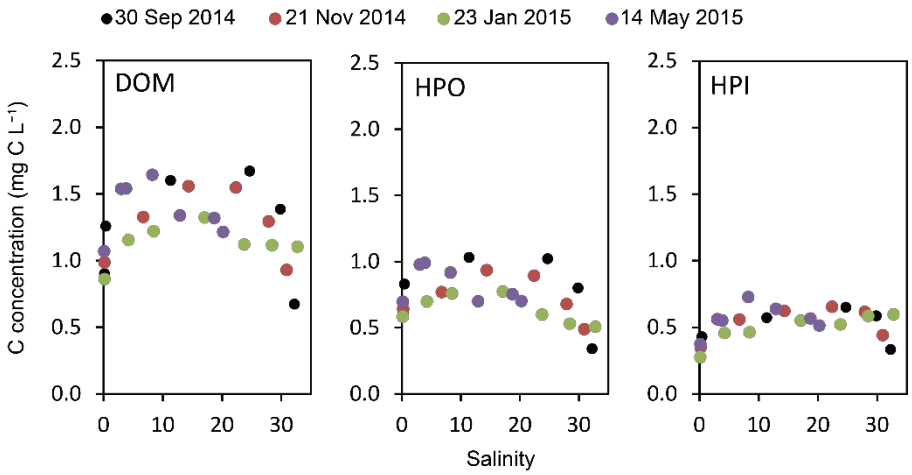

Figure S1. Dissolved organic matter (DOM) and hydrophobic and hydrophilic fraction of DOM (HPO and HPI) concentrations plotted along salinity.

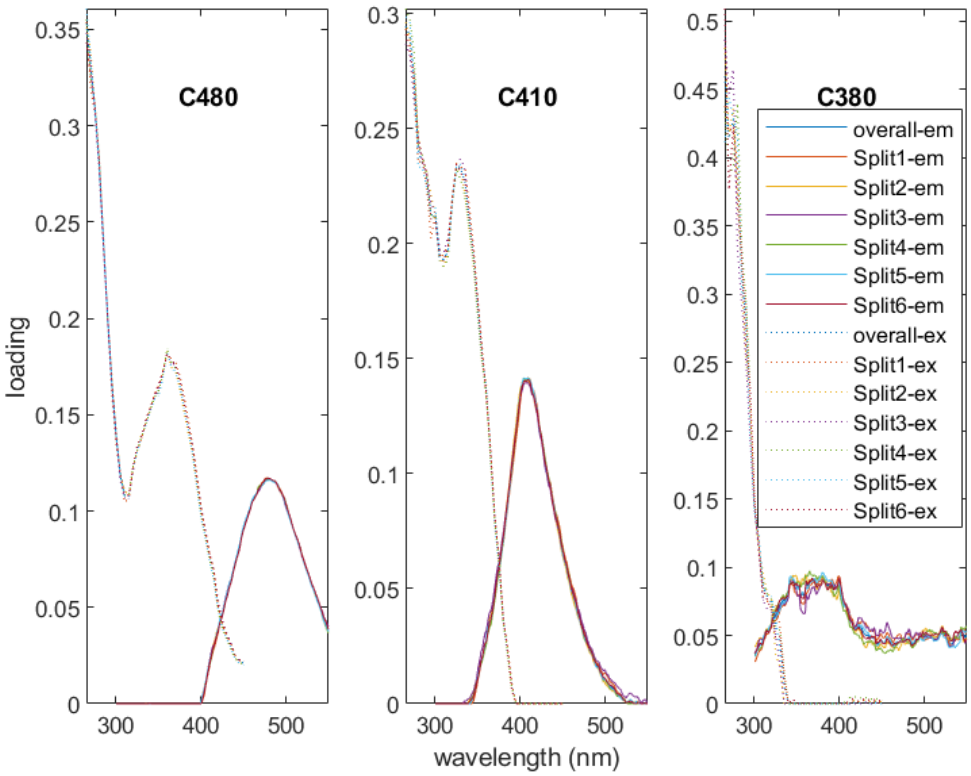

Figure S2. Loadings of excitation and emission spectra of the identified PARAFAC components (*overall-ex* and *overall-em*) and the result of split-half analysis (*Split1–6*). The dotted and solid curves represent excitation and emission spectra, respectively.

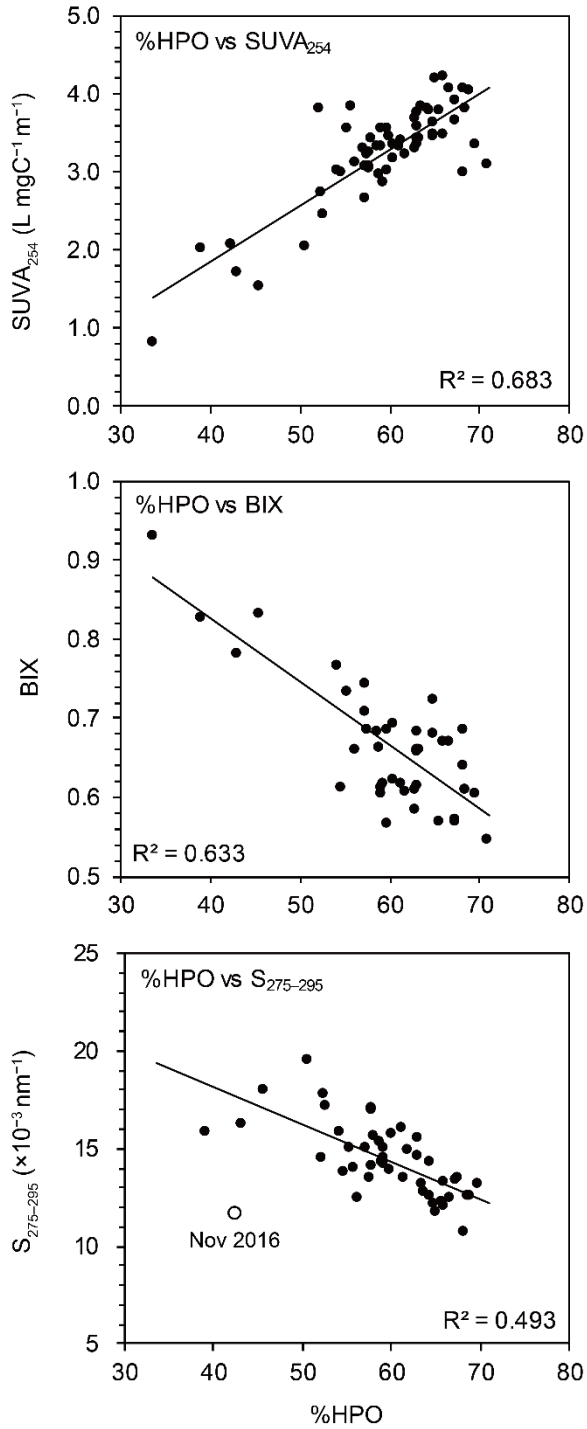

Figure S3. Relationships between the amount of hydrophobic fraction of DOM (%HPO, on carbon basis) and specific ultraviolet absorbance ($SUVA_{254}$), biological index (BIX), and spectral slope determined between 275 nm and 295 nm ($S_{275–295}$) for the Fukido River. The relationship between %HPO and $S_{275–295}$ was analyzed excluding an outlier (seawater sample collected in November 2016, represented by a white circle).

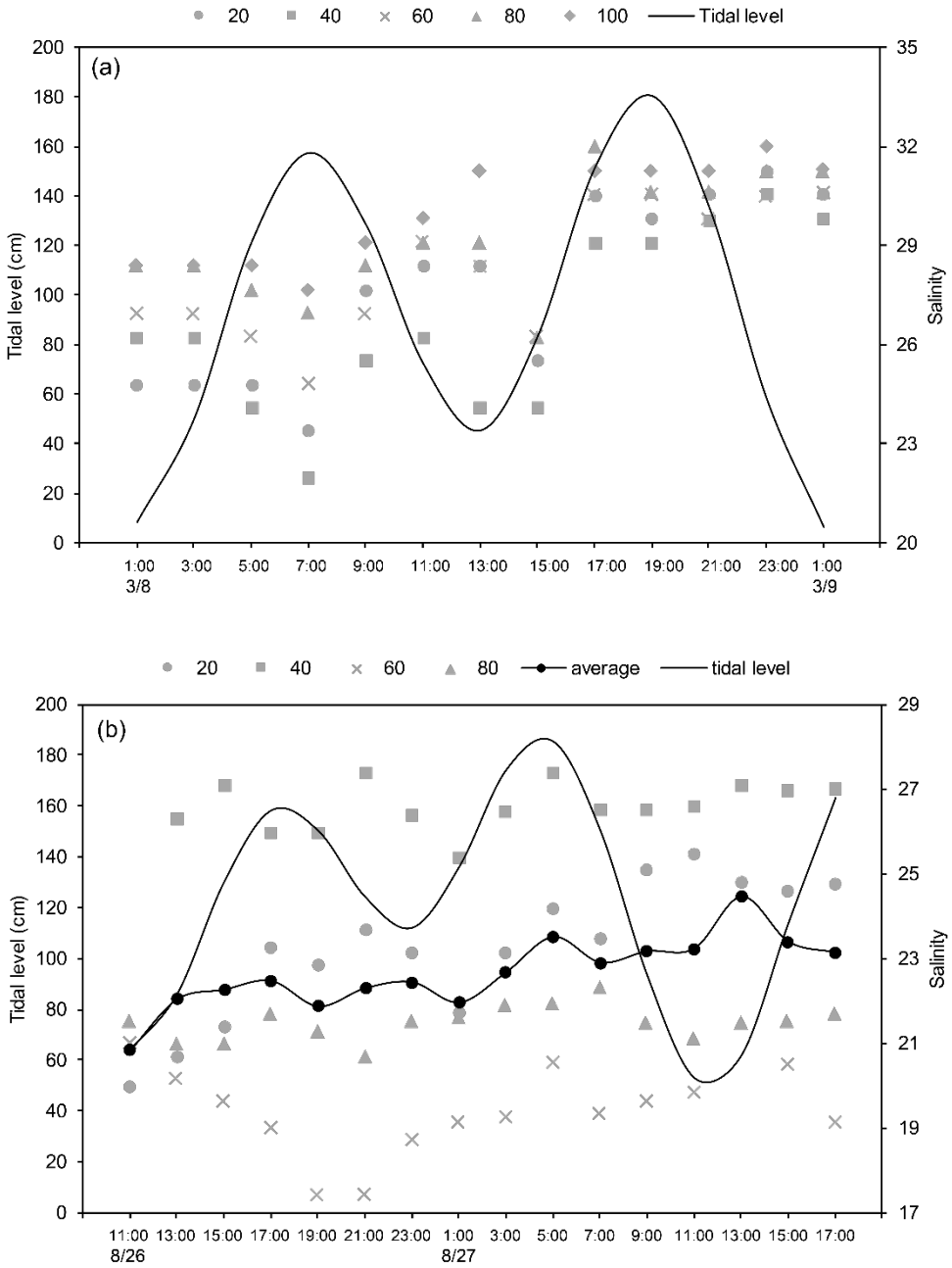

Figure S4. Groundwater salinity on (a) 8 March 2016 under the baseflow condition and (b) 26–27 August 2015 three days after Typhoon Goni. Average salinity values are presented for 26–27 August 2015 sampling to make the salinity trend clear. Black solid line represents the tidal level. Note the difference in y-scale for salinity.